Materials Today Bio 29 (2024) 101236

Contents lists available at ScienceDirect

Materials Today Bio

journal homepage: www.journals.elsevier.com/materials-today-bio

# Platelet interaction and performance of antibacterial bioinspired nanostructures passivated with human plasma

Anouck L.S. Burzava [a,b,*], Agnieszka Zuber [a], Andrew Hayles [a,c], James Morel [d], Richard Bright [a,c], Jonathan Wood [a], Dennis Palms [a,c], Dan Barker [e], Toby Brown [e], Krasimir Vasilev [a,c,**]

[a] STEM, University of South Australia, Mawson Lakes, South Australia, 5095, Australia
[b] Laboratoire Softmat, Université de Toulouse, CNRS, UMR 5623, Université Toulouse III – Paul Sabatier, 31062, Toulouse, France
[c] College of Medicine and Public Health, Flinders University, Bedford Park, 5042, South Australia, Australia
[d] School of Chemical Engineering, UNSW Sydney, New South Wales, 2052, Australia
[e] Corin Australia, Pymble, New South Wales, 2073, Australia

ARTICLE INFO

*Keywords:*
Bioinspired materials
Nanostructures
Antimicrobial
Platelet compatibility
Implants

ABSTRACT

The ever-increasing ageing of the world population is demanding superior orthopedic devices. Issues such as implant infection, poor osseointegration, or chronic inflammation remain problematic to the lifespan and long-term efficacy of implants. Fabrication of materials with bioinspired nanostructures is one emerging antibacterial strategy to prevent implant infection, however their interactions with blood components, and whether they retain their bactericidal properties in an environment displaying a complex protein corona, remains largely unexplored. In the present study, titanium alloy, commercially pure and plasma-sprayed titania were hydrothermally etched, passivated with human native plasma to develop a protein corona, and then incubated with either *Staphylococcus aureus*, *Pseudomonas aeruginosa* or human platelets. Surface analysis was first used to characterize the topography, chemical composition or crystallinity of each material. Fluorescence staining and SEM were performed to evaluate the nanostructure bactericidal properties, as well as to study platelet attachment and morphology. Composition of platelet supernatant was studied using ELISA and flow cytometry. Overall, our study showed that the bioinspired nanostructured surfaces displayed both impressive antibacterial properties in a complex environment, and a superior blood biocompatibility profile in terms of platelet activation (particularly for titanium alloy). Additionally, the amount of pro-inflammatory cytokines released by platelets was found to be no different to that found in native plasma (background levels) and, in some cases, presented a more pro-healing profile with an increased secretion of factors such as TGF-β, PDGF-BB or BMP-2. The nanostructured surfaces performed equally, or better, than hydroxyapatite-coated titanium which is one of the current gold standards in orthopedics. Although further *in vivo* studies are required to validate these results, such bioinspired nanostructured surfaces certainly show promise to be safely applied to medical device surfaces used in orthopedics and other areas.

## 1. Introduction

With the considerable scientific and technological advances made in the past decades, persons aged 65 or over have outnumbered children under five years of age worldwide for the first time in human history [1]. This trend is predicted to at least double in the coming years, exacerbating the burden caused by illnesses associated with old age. Joint failure is one such burden. As a result, the global market for orthopedic implants is forecasted to grow from USD 50 billion in 2022 to USD 72 billion by 2030, highlighting the unprecedented need for new biomaterials and technologies [2,3]. Current implants still suffer from several pitfalls, including infection, poor long-term osseointegration, or chronic inflammation [4–7]. Extensive research has been undertaken to prolong the lifespan and efficacy of the implanted materials in the

* Corresponding author. Laboratoire Softmat, Université de Toulouse, CNRS, UMR 5623, Université Toulouse III – Paul Sabatier, 31062, Toulouse, France.
** Corresponding author. College of Medicine and Public Health, Flinders University, Bedford Park, 5042, South Australia, Australia.
*E-mail addresses:* anouck.burzava-hopkins@cnrs.fr (A.L.S. Burzava), krasimir.vasilev@flinders.edu.au (K. Vasilev).

https://doi.org/10.1016/j.mtbio.2024.101236
Received 15 May 2024; Received in revised form 2 September 2024; Accepted 7 September 2024
Available online 14 September 2024

ultra-complex biological environment that is the human body, leading to the apparition of a new class of multifunctional materials in recent years. One emerging strategy is to fabricate nanoscale protrusions inspired by the structures found on insect wings. These surfaces kill bacteria on contact by mechanical forces, and have thus been referred to as 'mechano-bactericidal'. This phenomenon was first described by Ivanova and later translated to various materials including silicon and titanium [8–10]. In particular, titanium nanostructures have shown remarkable killing efficacy against a range of pathogens and have also recently been shown to promote strong bone integration in an ovine model [10–14]. Despite these impressive *in vitro* findings, little is known about how these novel materials interact with blood, or whether their bactericidal activity remains effective following exposure to blood or its components. The evaluation of the biocompatibility of blood-contacting devices is a necessary part of satisfying the ISO10993 standard, which is required to obtain FDA approval to release a medical device into the market [15,16]. A wide range of parameters are required to be below a certain threshold for a given material to be considered as "blood compatible" (i.e., not leading to substantial adverse reactions). Platelet activation is one of these key indicators, as an implanted material is immediately covered by plasma proteins, closely followed by the adhesion of platelets (within about 180 ms) [17].

Platelets are small cell fragments that play a crucial role in thrombosis and homeostasis [18]. Activated platelets are known to release numerous potent factors, including β-thromboglobulin or platelet-derived growth factor, and as such they constitute a cornerstone of blood response to a foreign material [19]. Platelet behavior has been shown to be directly influenced by the chemistry, surface energy, crystallinity, and topography of biomaterials [20–26]. Kammerer et al. for instance, showed that rougher surfaces promoted activation [27], while Zhang et al. demonstrated that the crystallinity of titania nanotubes had a significant impact on platelet adhesion and activation [28], and Hong et al. reported that hydrophilic modifications increase thrombogenic responses [29]. However, both Smith et al. and Yang et al. have shown that titania nanotubes were more blood-compatible than the smooth titanium control [30,31]. Interestingly, in the case of orthopedic implants, some level of platelet activation has also been found to be favorable to the osseointegration of the device and its long-term performance [32,33]. A consensus has therefore not yet been reached regarding what surface properties most contribute to platelet activation, and which outcome is most favorable when designing orthopedic implants. Overall, one can assume that if some level of platelet activation could indeed be favorable to bone healing, it would not be safe for a material to elicit an over amplified, generalized blood activation.

In this work, we therefore began by investigating whether the antibacterial activity of a nanostructured titanium surface would remain effective in more complex conditions, i.e. following exposure to human plasma. Then, we evaluated one of the primary aspects of blood-compatibility, platelet interaction towards a foreign material. In particular, how they may be directly impacted by the presence of titanium nanostructures, but also what would be the overall consequences of this platelet interaction for the surrounding biological environment by evaluating the effect of the cytokines produced by the platelets on macrophages (inflammation) and bone-marrow-derived mesenchymal stem cells (osseointegration).

## 2. Results

### 2.1. Characterization of HTE nanostructure surfaces

Let's start with considering a hip implant. This devices are commonly composed of the following parts: a femoral stem, a femoral head and an acetabular shell. All three components are usually made of titanium alloy (Ti6Al4V) due to the material high mechanical strength, comparatively low density, good osseointegration and superior corrosion resistance compared to other metal alloys [34,35]. As an additional step, commercially pure titanium can be plasma sprayed onto specific sections of the implants (i.e. where the implant is in direct contact with the femur or the pelvis) to enhance osseointegration properties by creating a rougher and more biocompatible interface [36–38]. An additional layer of hydroxyapatite can also be apposed to further improve bone remodelling and implant fixation [39–41]. The different metallic sections of a hip implant and their most common composition are presented in Fig. 1A. To fabricate bioinspired nanostructures with antimicrobial properties on clinically relevant materials, titanium discs were etched via an alkaline hydrothermal treatment using a 1M KOH solution (HTE-Ti). This etching process was applied to a representative range of titanium discs to model the different sections of a hip implant, namely Ti6Al4V alloy (Alloy), commercially pure titanium (CP), commercially pure titanium plasma sprayed onto titanium alloy (Sprayed), and hydroxyapatite-coated titanium (HA). The unmodified control surfaces (CTL) and their hydrothermally etched counterpart "HTE-Ti" are presented in the scanning electron microscope (SEM) images in Fig. 1B. All the HTE-Ti surfaces presented the characteristic sharp disordered titanium nanostructures, while the CTL samples appeared relatively smooth (only showing some pits and scratches from the machining and polishing steps during the manufacturing process. The hydrothermal etching process generated nanostructures with similar dimensions across the different titanium types (Table 1), with heights of approximately 350 nm, widths of 50 nm and average spacing of 250 nm between tips. The surface area, measured by atomic force microscopy (AFM), showed an increase of almost two-fold following the etching process for both Ti-alloy and CP. It was not possible to directly measure the surface area for the plasma sprayed samples due to limitations of the instrument, however, its value can be expected to be comparatively greater than that shown on the non-sprayed samples due to the micro-scale topography generated by the plasma spray process. The elemental composition of the outermost 10 nm layer was measured using X-ray photoelectron spectroscopy (XPS; Fig. 1C). Survey spectra consistently showed a significant increase in the oxygen content after hydrothermal treatment ($p < 0.05$), which is expected due to the thickening of the titanium oxide layer elicited by the process. In parallel, the etching process also removed surface contaminants, such as adventitious carbon, nitrogen or silicon, that are naturally introduced through the manufacturing process of the discs. This also resulted in proportionally increased percentages of titanium within the 10 nm outermost surface sections sampled by XPS. As expected, low levels of vanadium and aluminium were detected for the titanium alloy controls but not on any of the other surfaces (except traces of residual aluminum still visible from the polishing process). Interestingly, the hydrothermal etching process also led to an increase in the proportion of potassium, which can be attributed to the use of KOH as the etchant [42]. The percentage of potassium was significantly higher on plasma sprayed HTE, followed by commercially pure HTE, and finally on alloy HTE. The increased proportion of potassium on the plasma sprayed samples can be explained by the microtopography of the surface, as XPS solely measures the atomic composition of the first 10 nm of surfaces. However, it is also interesting to note that CP titanium tended to incorporate more potassium than alloy titanium. This could be due to a combination of slightly different surface charges and crystallinity. Finally, the chemical composition of HA-coated titanium ($Ca_{10}(PO_4)_6(OH)_2$) was confirmed, with oxygen, calcium and phosphorus being the principal elements detected. Additionally, a non-negligible amount of silicon was observed for these surfaces, which was likely residual from the silica gel that was used as crystallizing medium [43,44]. Wettability measurements were also performed on the titanium surfaces, revealing a water contact angle of $<10^\circ$ on all hydrothermally etched samples, indicating a highly hydrophilic surface. Sprayed-CTL samples were particularly hydrophobic, with a contact angle of approximately 150°, which can be explained by the additional presence of microscopic air pockets locked within the microporous topography (Fig. 1D and S1) [45]. Grazing angle x-ray diffraction (GA-XRD) was then performed to investigate whether any changes in

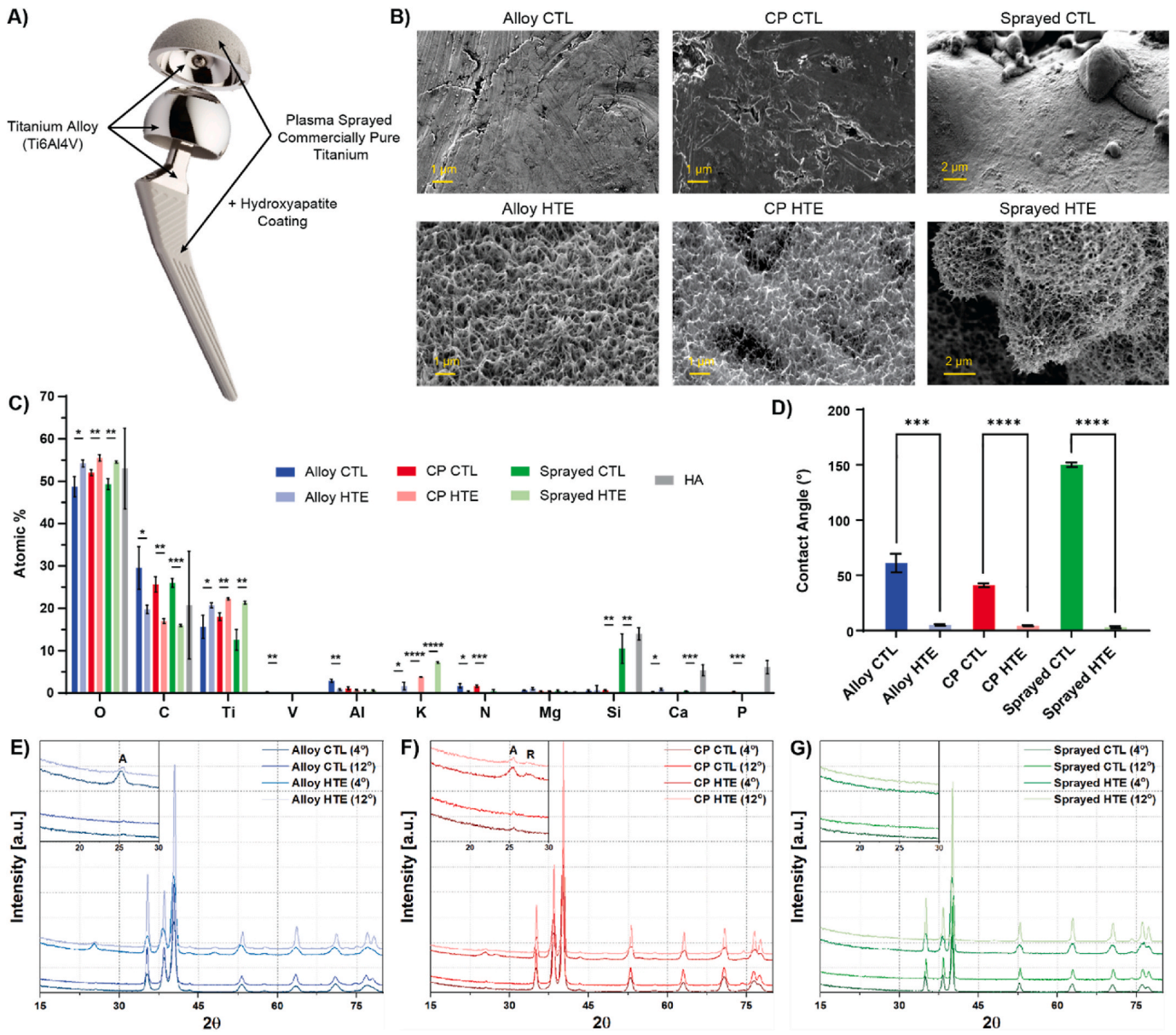


**Fig. 1.** Surface characterization of the different titanium substrates, before and after hydrothermal etching. A) Hip implant showing localization of the substrates of interest. B) Representative SEM images (stage tilted at 45°). C) XPS elemental composition obtained from survey spectra ($n = 3$, mean ± SD). D) Water contact angle analysis ($n = 3$, mean ± SD). E-G) Representative GAXRD depth profiles of CTL versus HTE for E) titanium alloy, F) commercially pure titanium, and G) plasma sprayed titanium. "A" and "R" in the zoomed-in section indicating anatase and rutile peaks respectively. Multiple t tests comparing HTE-Ti vs unmodified substrates ($^*p < 0.05$; $^{**}p < 0.001$; $^{***}p < 0.001$ and $^{****}p < 0.0001$).

crystallinity could be observed (Fig. 1E–G). For both alloy and CP discs, the unetched controls showed a minor presence of titanium oxide in the form of anatase. The natural oxide layer of titanium grows to a thickness of between 3 and 7 nm, hence only traces are expected to be detected with the potential for some of the surface oxides to remain undetected due to the GA-XRD crystal size detection limit of 3 nm [46–48]. Following hydrothermal treatment, both alloy and CP discs showed a marked increase in the presence of titania, confirming that both samples underwent a thickening of the oxide layer as evidenced by characteristic peaks in the 2θ region between 25° and 28°. The oxide layer of CP HTE-Ti was composed of both anatase and rutile, as identifying peaks at 25.3° (ICDD 00-021-1272) and 27.4° (ICDD 00-021-1276), respectively, were detected. In comparison, alloy HTE-Ti surfaces showed no evidence of rutile formation, but a greater proportion of anatase was present relative to the bulk titanium peaks. This highlighted a trend towards anatase formation for the titanium alloy samples. Despite these changes in titanium crystallinity observed for smooth substrates, no discernible change was observed for samples that were plasma sprayed with CP titanium. In that case, the detection of the oxide layer via GA-XRD was prevented due to the disruption caused by the micro-undulation of the overall surface, a property that extended below the calculated x-ray penetration depth of 2 μm and 5 μm for an angle of incidence of 4° and 12°, respectively. Taken together, these variations in surface topography, area, chemistry, and crystallinity, are expected to influence the identity, quantity and conformation of adsorbed proteins that will attach upon implantation [49,50]. Forming what is called a protein corona, these proteins will essentially confer a new biological identity to each surface, which will guide the subsequent bio-interfacial interactions [51–53].

**Table 1**
Surface characterization analysis. Surface area measured using AFM from a 20 μm × 20 μm scanning area. Measurement of nanostructures length, width and spacing calculated from SEM images (for height and width $n = 180$ and for spacing $n = 18$, mean ± SD). * values were determined in earlier work published by Hayles et al. (2022) [54].

| Surface characterization | Alloy CTL | Alloy HTE | CP CTL | CP HTE | Sprayed CTL | Sprayed HTE |
|---|---|---|---|---|---|---|
| Surface area ($\mu m^2$) | 417.3 | 700.1 | 439.7 | 800.7 | NA | NA |
| Nanostructure height (nm) | – | 405 ± 122 | – | 296 ± 48 * | – | 390 ± 84 |
| Width at mid-height (nm) | – | 37 ± 14 | – | 62 ± 12 * | – | 37 ± 12 |
| Distance between spikes (nm) | – | 220 ± 29 | – | 287 ± 9 * | – | 226 ± 24 |

### 2.2. Bacterial viability analysis

HTE-Ti has been documented to have numerous interesting properties, such as contact-killing bacteria, inhibiting bacterial and fungal biofilm, and enhancing antibiotic efficacy [10,11,55,56]. However, little is known about nanostructure antibacterial efficacy following exposure to human plasma. Following surgical placement, medical device surfaces come in direct contact with blood, which is composed of 55 % plasma and contains thousands of proteins. To confirm that the HTE-Ti surfaces retained their antibacterial properties following incubation with human plasma, surfaces were incubated with either Gram-positive *Staphylococcus aureus* (*S. aureus*) or Gram-negative *Pseudomonas aeruginosa* (*P. aeruginosa*) for 18 h. Live/Dead fluorescence imaging (Fig. 2A and C) showed that all HTE samples were effective at killing both species. A comparatively greater bacterial load was observed on the sprayed CTL compared to the alloy-CTL and CP-CTL, likely due to its micro-scale topography. However, this effect was reversed by the HTE process, with viabilities dropping from 99.2 % to 32.2 % for *S. aureus* ($p < 0.0001$), and from 99.3 % to 5.1 % for *P. aeruginosa* ($p < 0.0001$). Interestingly, the HA control surface appeared particularly favorable to bacteria colonization, with both *S. aureus* and *P. aeruginosa* arranged into discernible aggregates. This suggests that the HA surface, although known to improve osseointegration, may also facilitate biofilm formation [57,58]. Antibacterial efficacy was determined using Live/Dead staining (Fig. 2B and D), which yielded a viability of 35 % for *S. aureus* and 5 % for *P. aeruginosa* for all HTE samples, compared to >90 % for all untreated titanium samples. This is comparable to the values reported in other studies where the surfaces had not been passivated with human plasma, suggesting that the protein corona had little impact on the antibacterial properties of the HTE-Ti surface [12,13]. SEM images also reveal that the sharp nanostructures on the HTE-Ti surfaces retained their antibacterial potency after passivation with human plasma, with the bacterial membrane appearing deformed and deflated as evident from the SEM images in Fig. S2. These images, together with the viability data, further corroborate the contact-killing mechanism theory that has been put forward by others, as the primary mechanism behind the antibacterial properties of the HTE-Ti surface [59–61].

### 2.3. Platelet adhesion and morphology analysis

Given the ability of these titanium nanostructures to kill bacteria, it is natural to question whether they would have any detrimental effects

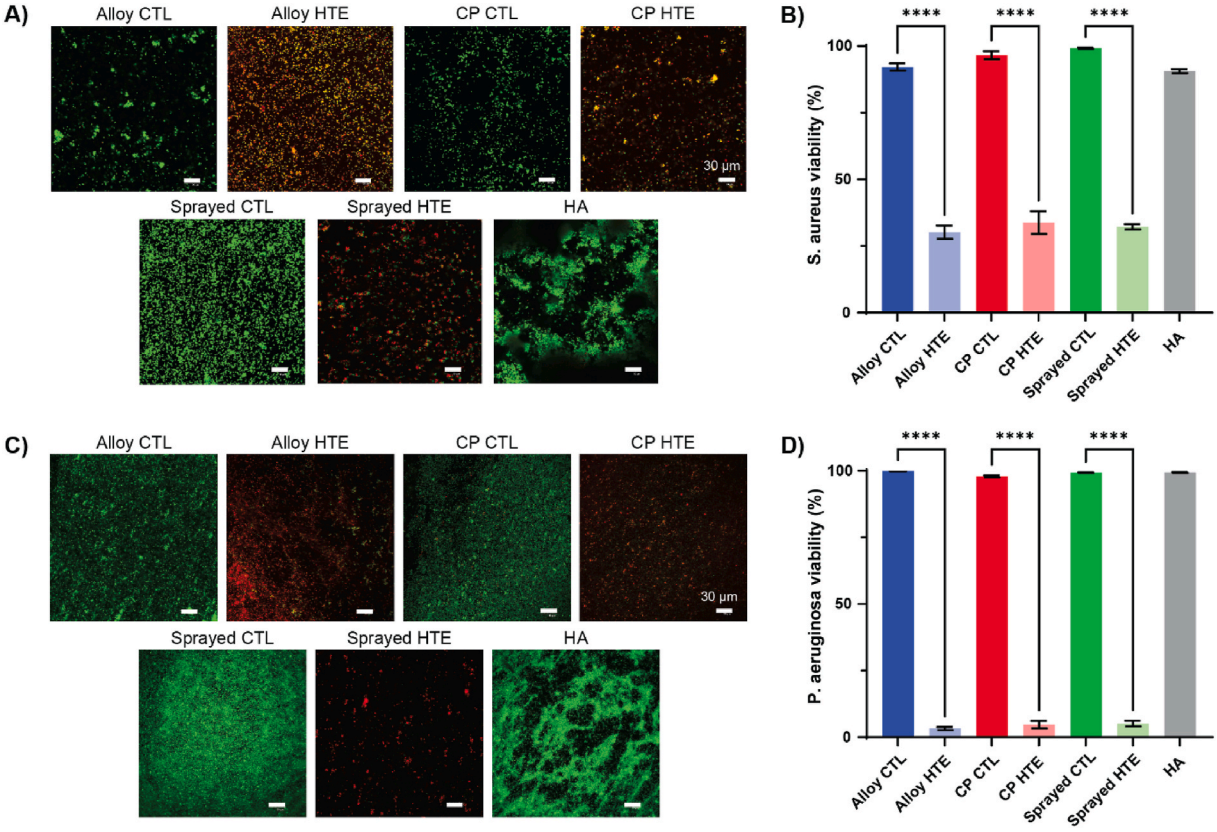


**Fig. 2.** Bacteria killing on plasma passivated surfaces, with live-dead staining and corresponding viability percentages for A-B) a Gram-positive bacterial species (*S. aureus*) and C-D) a Gram-negative bacterial species (*P. aeruginosa*). Dead bacteria appear in red, while live bacteria appear green. Scale bar represents 30 μm. Graphs show $n = 4$, mean ± SEM. One-way ANOVA with Tukey's multiple comparison tests (****$p < 0.0001$).

on platelets, possibly triggering blood activation cascades and leading to inflammation. Platelets are small cellular fragments that play a crucial role in thrombosis and hemostasis. Following the adsorption of plasma proteins on an implanted biomaterial, platelets are amongst the first on-site and constitute a cornerstone of the inflammatory response to a foreign material [17]. Although some level of platelet activation could be favorable to bone healing, it would not be safe for a material to elicit an over amplified blood activation (i.e. leading to persistent inflammation and eventually implant rejection) [32,33]. Platelets were collected from three healthy blood donors and incubated for 2 h on the different titanium surfaces in independent experiments. Collagen I and tissue culture plate control (TCPS) were added as positive and negative controls (respectively) for platelet activation. Platelet morphologies were also recorded, as they strongly correlate with their activation state. Activated platelets present a spread and spindle-like morphology, when they are otherwise small and round in their non-activated state. Representative images of platelets morphologies are presented in Fig. 3A, while Fig. 3B shows the total number of platelets that attached to the surfaces, along with the proportion of each morphology subset. Surprisingly, the addition of nanostructures had little impact on platelet behavior overall, and didn't lead to a major increase in platelet attachment and/or spreading. In fact, all the titanium substrates showed significantly fewer platelets spreading compared to the collagen I (which is known to activate platelets), with 61 % of platelets displaying a spread morphology on the collagen I versus only 2–8% on the titanium surfaces (details available in Table S1). The total number of platelets attached was also significantly lower than on collagen I, with the exception of the plasma-sprayed samples (Table S2). This can be explained by the substantial difference in surface area due to the presence of microtopography on these substrates. The fact that the percentages of each morphology subset remained essentially the same as what was observed on the smooth titanium further corroborates that hypothesis. Furthermore, the total number of platelets attaching to the alloy and CP titania (with or without the addition of nanostructures) was inferior or equal to that measured on the TCPS, which is known to be biologically inert and thus a good negative control for activation of blood cascades. Percentages of each morphology subset were also in the same ranges, indicating that all surfaces triggered an equal degree of platelet activation. Interestingly, the HA-coated titanium showed the highest total number of platelets attached, and displayed spread/dendritic morphology percentages close to those observed on the collagen I positive control (56.9 % and 85.3 % respectively). This could be explained by a combination of a) an increased surface area due to the microtopography and b) the presence of calcium and phosphate which are known to be intricately linked to platelet activation. In terms of the direct influence of the nanostructures on platelet attachment and spreading, smaller differences were noted. For instance, although slightly more platelets attached to the hydrothermally etched surfaces compared to their smooth controls for CP and sprayed titania, the opposite was observed for titanium alloy. While the increase in surface area on the HTE-Ti surfaces could explain why more platelets attached to these surfaces, it is surprising that the etching appears to render the titanium alloy more inert towards platelets. One reason could be that the increased titanium oxide layer on the etched surfaces may help prevent some residual cytotoxic ions from leaching. It is also possible that the difference in titania crystallinity observed via GA-XRD, with alloy HTE-Ti discs predominantly presenting anatase phase while CP HTE-Ti discs displaying a mixture of anatase and rutile, had either a direct impact on platelet attachment or an indirect effect by possibly impacting the nature of the protein corona forming on the discs [62,63].

SEM imaging was then performed to further examine how the platelets were interacting with the different surfaces (Fig. 4). First and foremost, the titanium nanostructures were still clearly visible, meaning the passivation of the HTE-Ti surfaces with human plasma did not result in their masking. This is consistent with the fact that the HTE-Ti surfaces retained their bactericidal properties, and also confirms that the nanostructures were in direct contact with the platelets. Most surprisingly, however, the HA substrate appeared covered by a dense fibrin network, suggesting this surface triggered the activation of clotting cascades upon contact with human plasma. This phenomenon can likely be explained by the release of $Ca^{2+}$ and $H(PO_4)^{2-}$ ions into the media, which are known to be a potent inducer of fibrin monomer polymerization and to strengthen the structure of the fibrin network [64–67]. Fibrin is also recognized as a substrate to which platelets are strongly adherent, leading to their activation and spreading [68,69]. Distinctive spread and dendritic platelet morphologies were indeed confirmed on the HA substrate via SEM, which aligns with published literature [70]. Platelets otherwise remained predominantly round on the titanium surfaces, even when direct contact with the nanostructures was observed. As expected, platelets extensively spread onto the collagen I-coated positive control

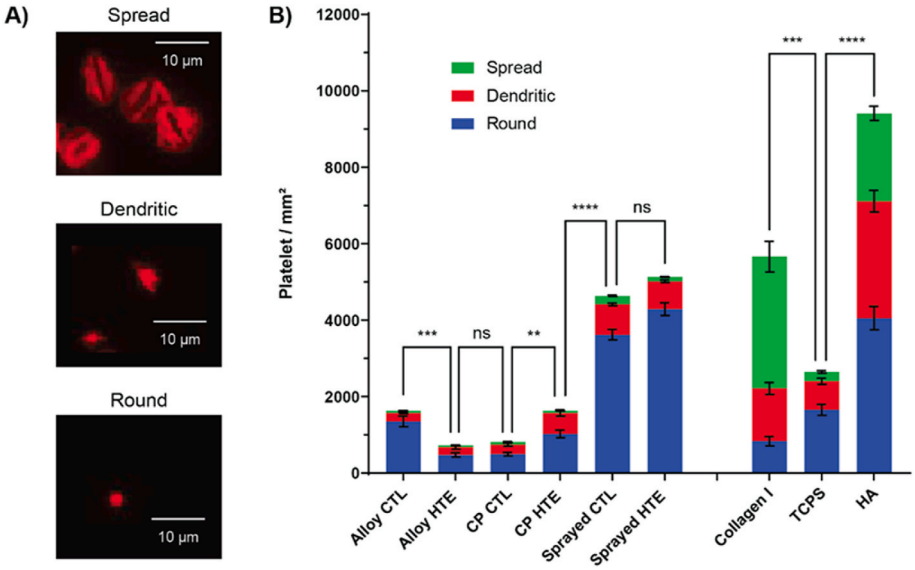


**Fig. 3.** Platelet interaction with the HTE-Ti surfaces, with A) representative images of the different platelet morphologies using phalloidin staining (cytoskeleton in red) and B) platelet number and morphology attached to the different surfaces after 2 h incubation (3 donors combined, n = 81, showing mean ± SEM). One-way ANOVA with Tukey's multiple comparison test performed on platelet total count (*$p < 0.05$; **$p < 0.001$; ***$p < 0.001$ and ****$p < 0.0001$).

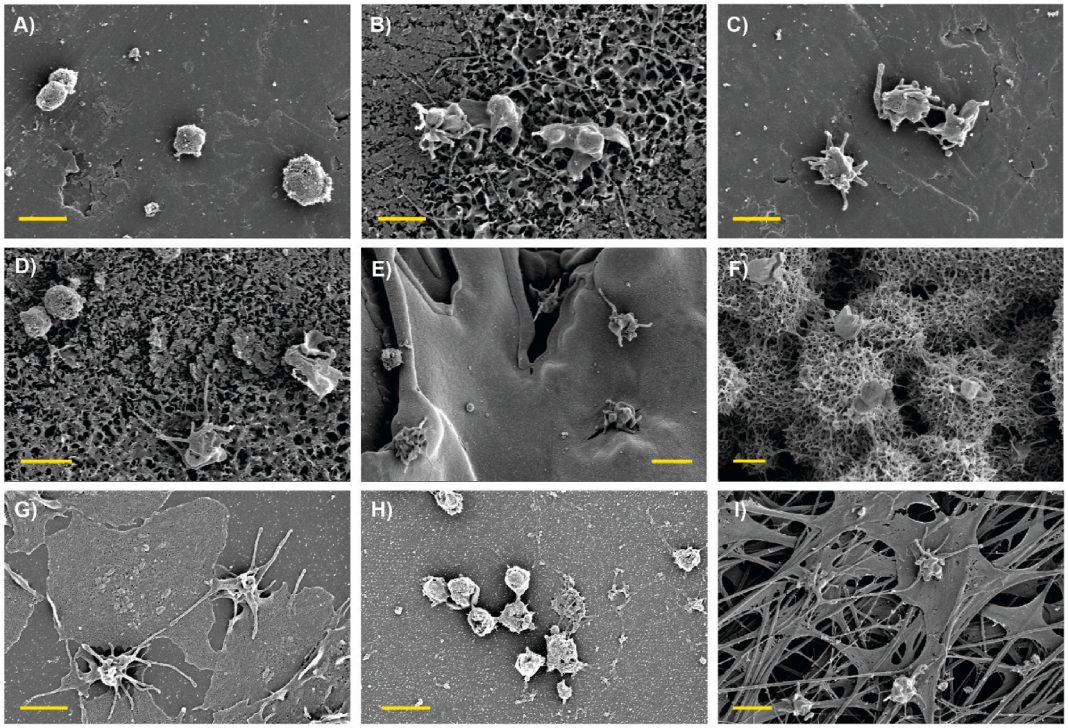


**Fig. 4.** SEM images of human platelets attached to the different surfaces after 2 h incubation, with: A) Ti alloy CTL, B) alloy-HTE, C) CP-CTL, D) CP-HTE, E) Sprayed-CTL, F) Sprayed-HTE, G) Collagen I coated control, H) TCPS control and I) HA-Ti. Scale bar = 2 μm.

but remained round on the TCPS negative control, meaning that platelets expressed normal behavior following their isolation from blood and did not appear to be artificially activated through that process.

### 2.4. Platelet activation analysis

Overall, it appeared that the addition of nanostructures to titanium did not trigger excessive platelet adhesion and/or lead to major morphological changes. However, these observations only remain indirect/early indicators of platelet activation. It is also important to measure the end-product of these activations, with the secretion of potent cytokines and the recruitment of immune cells to the inflamed site being the actual end-product of these activation cascades.

A wide range of ELISA assays were therefore performed on the platelet supernatant collected after the 2 h of incubation on the surfaces, to evaluate whether any of these cytokines were found in higher levels than in human plasma (baseline, a sample not containing any platelets). The first set of assays, presented in Fig. 5A–D, focused on factors known to predominantly have pro-inflammatory effects, including Platelet factor 4 (PF4), β-Thromboglobulin (β-TG), Thromboxane B2 (TxB2) and Thrombospondin 1 (TSP-1) [71–73].

PF4 is a potent CXC chemokine that is released from α-granules during platelet activation and plays an important role in wound repair and inflammation. It is closely associated with blood coagulation (prothrombotic) and tends to be found in high concentrations at sites of vascular injury [71,74]. Interestingly, only the platelets in contact with the alloy-CTL were found to secrete significantly more PF4 compared to the commercial native plasma control. This is in accordance with previous findings, that indicated that titanium alloy may be less inert than the other materials. Although platelets appeared to secrete slightly less PF4 when seeded onto the HTE-Ti surfaces compared to the unetched control, that difference was not found to be statistically significant, perhaps also due to the donor variability observed. Similar to PF4, β-TG (also known as CXCL7) is a potent CXC chemokine released from α-granules during platelet activation. It is a potent chemoattractant and activator of neutrophils, and has also been found to be a potential novel platelet-derived activator of coagulation FX [71,74]. While we observed a trend of platelets secreting less β-TG on unetched control compared to hydrothermally treated surfaces, these differences were again not statistically significant. Furthermore, none of the surfaces tested appeared to lead to the secretion of significantly more β-TG than what is found circulating in native plasma. Another pro-inflammatory factor of interest, TxB2, is actually an inactive stable metabolite of TxA2 (which is unstable and rapidly hydrolyzed into TxB2 in a physiological environment). TxA2 is a proinflammatory/prothrombotic eicosanoid released by activated platelets, and is the major arachidonic acid derivative originating from the cyclooxygenase (COX)-1 pathway. It was shown to be a potent vasoconstrictor and to lead to more platelet activation and aggregation [73,75]. Thromboxanes are also known to stimulate the production of ECM proteins, thereby contributing to fibrosis and scarring. Finally, studies found that TxA2 had direct immunomodulatory properties, such as the promotion of T cells proliferation [76,77]. In our study, platelets only secreted significantly higher levels of TxB2 when incubated on the HA-coated titanium. This correlates well with the spread/dendritic morphology that was observed for platelets on that substrate. Incubation on the other materials showed only marginally increased TxB2 levels to what was seen in commercial native plasma control, with slightly more TxB2 found for the-Ti compared to unetched surfaces (although the difference was again not statistically significant due to high donor variability). Finally, TSP-1 is a pro-thrombotic glycoprotein that is released from α-granules during platelet activation. TSP-1 also plays an important role in wound repair and inflammation. For instance, it is an important negative regulator of angiogenesis and bone cell differentiation (i.e. by activating TGF-β, and blocking NO accumulation), has a dose-dependent antiproliferative effect on fibroblasts, osteoblast and endothelial cells, and contributes to clot formation [78,79]. Interestingly, it has also recently been shown that TSP-1 associates/serves as an adhesion site for Gram-positive bacteria, thereby facilitating their environment colonization and escape from the immune system [80]. This protein showed the highest levels of contrast between the materials tested and the commercial native plasma control baseline of all the pro-inflammatory factors. All the surfaces,

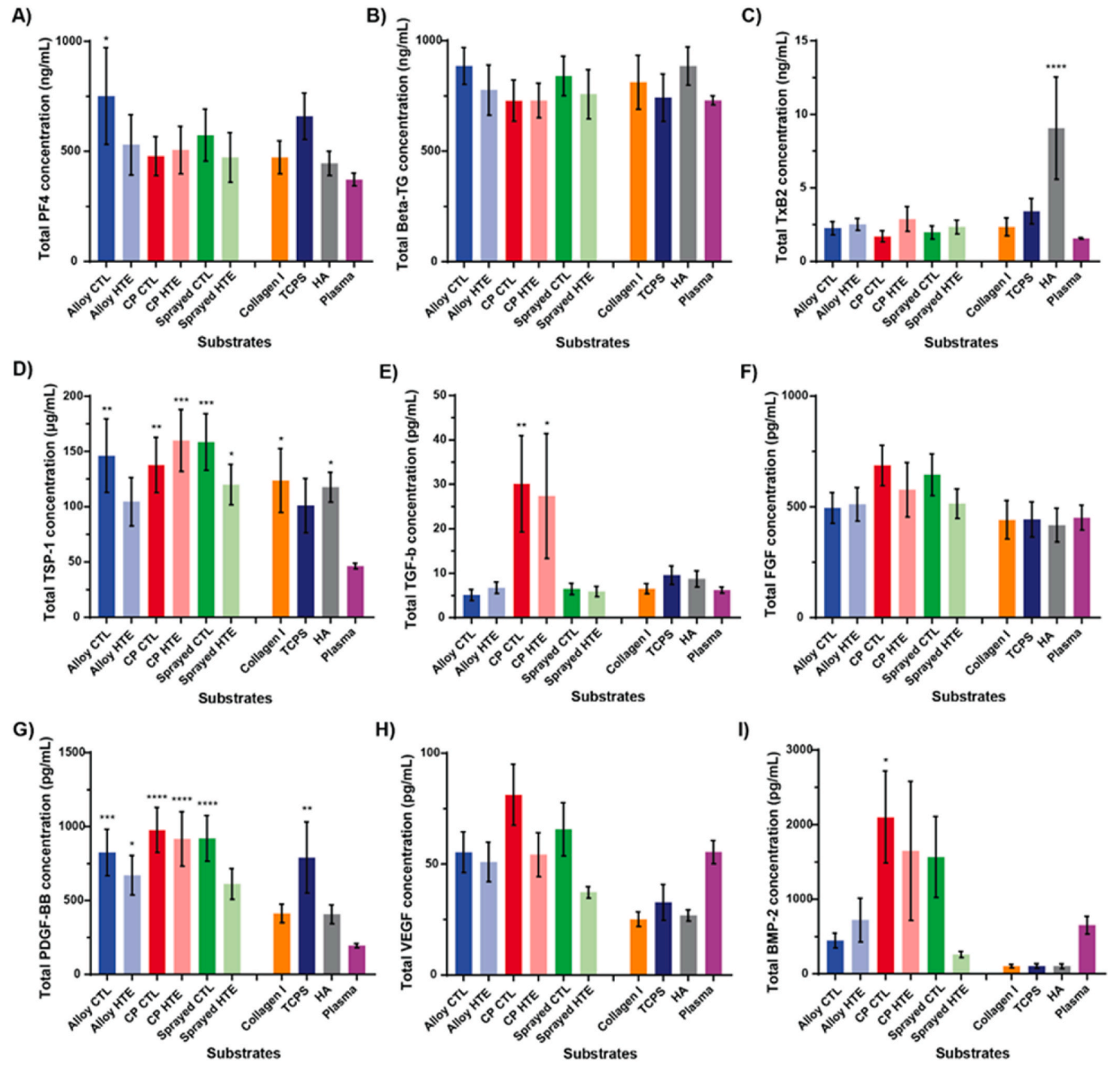


**Fig. 5.** Factors secreted by platelets over the 2 h incubation on the surfaces. (A–D) Pro-inflammatory factors found using ELISA and (E–I) pro-healing factors detected using flow cytometry. Showing mean ± SEM, $n = 6$ for A-D and $n = 12$ for E-I. One-way ANOVA with Dunnett's multiple comparison tests against Commercial Native Plasma control (*$p < 0.05$; **$p < 0.01$; ***$p < 0.001$ and ****$p < 0.0001$).

with the exception of alloy HTE and TCPS negative control, indeed showed significantly more TSP-1 in the supernatant than what was observed in native plasma. Overall, the presence of nanostructures did not lead to a substantial increase in the secretion of pro-inflammatory factors compared to unetched surfaces, with all the surfaces remaining biologically inert. Additionally, the HTE modification again seemed to make the alloy substrate more biocompatible towards platelets compared to the unetched material.

The second set of assays, presented in Fig. 5E–I, focused on factors known to predominantly have pro-healing properties, including transforming growth factor–β (TGF-β), fibroblast growth factors (FGF), platelet-derived growth factor (PDGF-BB), vascular endothelial growth factor (VEGF) or bone morphogenetic protein (BMP-2). TGF-β and FGF are known to mediate wound healing, angiogenesis, ECM formation and immune response [81,82]. Only the commercially pure substrates showed a marked increased secretion of TGF-β compared to commercial native plasma, with 30.1 pg/mL for CTL and ($p = 0.004$) and 27.4 pg/mL for HTE-Ti ($p = 0.016$). Small changes were visible across the other surfaces, however, none of these differences were statistically significant. PDGF-BB is another important pro-healing factor, that was for instance shown to enhance the proliferation/migration of fibroblasts and general wound healing. All surfaces, apart from sprayed-HTE, collagen-I and HA surfaces, induced platelets to secrete significantly more PDGF-BB than the base level seen in commercial native plasma with:

alloy CTL at 824.9 pg/mL ($p = 0.0007$), alloy HTE at 670.5 pg/mL ($p = 0.028$), CP CTL at 977.6 pg/mL ($p < 0.0001$), CP HTE at 916.8 pg/mL ($p < 0.0001$), sprayed CTL at 919.8 pg/mL ($p < 0.0001$) and TCPS at 790.9 pg/mL ($p = 0.0015$). VEGF, which is a strong promoter of angiogenesis, wasn't secreted by platelets in amounts that were significantly different to the commercial native plasma for any of the materials tested. However, the levels of VEGF were generally higher for titanium substrates compared to the controls (collagen I, TCPS, or HA). CP-CTL and Sprayed-CTL were found to lead to the secretion of significantly more VEGF compared to the collagen-I surfaces ($p = 0.0003$ and $p = 0.16$ respectively), compared to the HA-coated titanium ($p = 0.005$ and $p = 0.02$ respectively). The CP-CTL also showed increased VEGF concentration compared to TCPS control ($p = 0.001$). Once again, the difference between the CTL and the HTE-Ti surfaces was not statistically significant for titanium alloy and CP, however, it was found that sprayed-HTE surfaces led to the secretion of slightly less VEGF than its unetched counterpart ($p = 0.03$). Finally, BMP-2, which is a potent osteogenic factor and therefore important in the context of orthopedic implants and osseointegration, was significantly secreted in greater amount by platelets that adhered to the CP-CTL compared to the commercial native plasma, with 2101.6 pg/mL ($p = 0.017$). Levels of BMP-2 also appeared generally more important for the alloy HTE, CP-HTE, and sprayed-CTL, however, that difference was not found to be statistically significant, possibly due to the high degree of donor variation. Both CP-CTL and CP-HTE surfaces were found to have significantly higher levels of BMP-2 compared to the HA surfaces ($p = 0.005$ and $p = 0.049$ respectively). In regards to pro-healing factors, PDGF-BB was the pro-healing factor secreted in the highest concentration, far above what was observed in commercial plasma. Titanium-based substrates therefore appeared to be generally associated with PDGF-BB secretion by platelets. Albeit differences between the different types of titania were most of the time quite minute, CP surfaces appeared to display a superior profile in terms of biocompatibility and rapid integration to host tissue. Surprisingly, even more so than the HA-coated titanium surface which is nowadays often used as a benchmark in terms of improved/accelerated osseointegration.

### 2.5. Impact of platelet secreted cytokines on macrophages and BMSCs

The analysis of platelet derived cytokines provides information about the interaction at the interface between platelets and the surface, and their effect on the local environment. To further probe how this would influence the host tissue in a clinical scenario, we studied the impact of the secreted cytokines from platelets on macrophages (to determine immunological reactions and inflammation) and bone-marrow-derived mesenchymal stem cells (BMSCs) (to assess the effect in osseointegration).

Macrophages are phagocytic cells that are able to recognize foreign substances (i.e. pathogens, biomaterial-derived particles or cellular debris) and then degrade them. As such, they are an essential component of both the immune and wound healing responses towards a foreign body. Depending on the factors detected by these cells and the characteristics of the environment, resting macrophages (M0) can polarize into two distinct sub-profiles: pro-inflammatory M1 or pro-healing M2. Although both types are known to co-exist during the initial inflammatory phase, the M1/M2 ratio is thought to be an important predictor of whether the material will successfully integrate into its biological environment long term [83–85]. Human M0 macrophages derived from a THP-1 cell line were therefore cultured for 7 days in media supplemented with 0.7 % of the platelet supernatant that was collected after 2 h culture on the surfaces. Additional control media were included, with a pro-inflammatory media containing 100 ng/mL LPS and 20 ng/mL INF-γ (known to promote M1 polarization); and a pro-healing media containing 20 ng/mL IL-4 and 10 ng/mL IL-10 (known to promote M2 polarization); and a negative control media "Normal media" that wasn't supplemented with platelet supernatant or additional growth factors. Fig. 6A shows the evolution of the viable cell number over the 7-days of culture. Across all media tested, macrophages appeared to maintain a steady cell number and to remain viable until day 3, then slowly start to decline at day 7. With the exception of the M1-inducing control media which lead to a statistically significant lower number of viable cells compared to "normal" unsupplemented media, all other culture media showed similar viability profiles. Looking at the factors produced by macrophages, interferon γ (IFN γ) and tumor necrosis factor α (TNFα) are some of the more potent inflammatory cytokines produced by this cell type [86,87]. On the other hand, CD11c and IL-10 are commonly recognized as representative markers of M1 and M2 polarization, respectively [88–90]. At day 3, the expression level of these key genes was thus analyzed using RT-PCR in order to obtain an indication of macrophages polarization (Fig. 6B). Platelet supernatants originating from culture on alloy-CTL and sprayed-CTL were the only materials tested that led to a significantly increased expression of inflammatory factors compared to the normal unsupplemented media, with 8.6 ($p < 0.0001$) and 5 ($p = 0.04$) fold change observed for TNFα respectively. Consequently, they were also the ones displaying the highest levels of CD11c expression (fold changes of 20.4 for alloy-CTL and 11.4 for sprayed-CTL), which is consistent with a trend towards pro-inflammatory M1 polarization. Platelets cultured on alloy-HTE, CP-CTL and sprayed-HTE titania discs also produced a supernatant that resulted in increased levels of CD11c expression in macrophages, although to a much lesser extent: ×9.5 ($p < 0.0001$), ×5.8 ($p = 0.008$) and ×6.7 ($p = 0.0008$) respectively. Expression levels of IL-10 following culture in supplemented media were not found to be significantly different to these observed in macrophage culture in unsupplemented normal media. These gene expression results would therefore indicate that alloy-CTL and sprayed-CTL may push macrophages towards a more pro-inflammatory M1 profile, while the others appear to remain at a resting M0 profile as they indicated no clear polarization towards either M1 or M2. Interestingly, HTE etching of the titanium alloy discs appeared to significantly reduce pro-inflammatory responses ($p = 0.0005$), which would be consistent with what was previously observed with platelet activation. To corroborate the gene expression results with actual marker expression on the macrophages, CD80 and CD163 fluorescence staining were performed on the cells throughout their culture to evaluate M1 and M2 profiles, respectively (Fig. 6C and **D**). Surprisingly, levels of CD80 markers across all materials were similar to these observed on unsupplemented control media for each time point. This would indicate that although there was a trend in gene expression towards M1 polarization for some of these surfaces (i.e. alloy-CTL and sprayed-CTL), they are not sufficient to lead to a clear shift in the cell expressed markers at the concentration of supernatant used in this study. Furthermore, the levels of CD163 (M2 profile) were higher than normal media for titanium alloy-CTL, CP-HTE, collagen I and HA surfaces on day 1, but then levelled out by day 7, indicating a very transient initial effect. At day 7, however, solely the sprayed-CTL discs showed a statistically significant increased expression of M2 marker CD163 compared to normal media ($p = 0.007$). Although the gene expression results on day 3 suggest that this material would be trending more towards a pro-inflammatory profile, the actual marker expression showed a shift towards the M2 profile on day 7.

Perhaps an enhanced/exacerbated initial inflammation state rapidly resolved to a more pro-healing state. Finally, the macrophage production of a range of cytokines was evaluated to further comprehend the impact of platelet supernatant on macrophage polarization and the possible pro-inflammatory or pro-healing cascades being triggered as a result. Flow cytometry was used to follow the levels of key cytokines secreted over time, namely: TNF-α, IFN-γ, IL-1β or IP-10 (associated with pro-inflammatory states); and IL-4 or IL-10 (considered to be more pro-healing factors) [91]. Fig. 6E shows that if the levels of pro-inflammatory cytokines were much higher in the control M1 media, very little differences were observed in the other media. Platelet supernatant from the HA surfaces resulted in increased secretion of IFN-γ

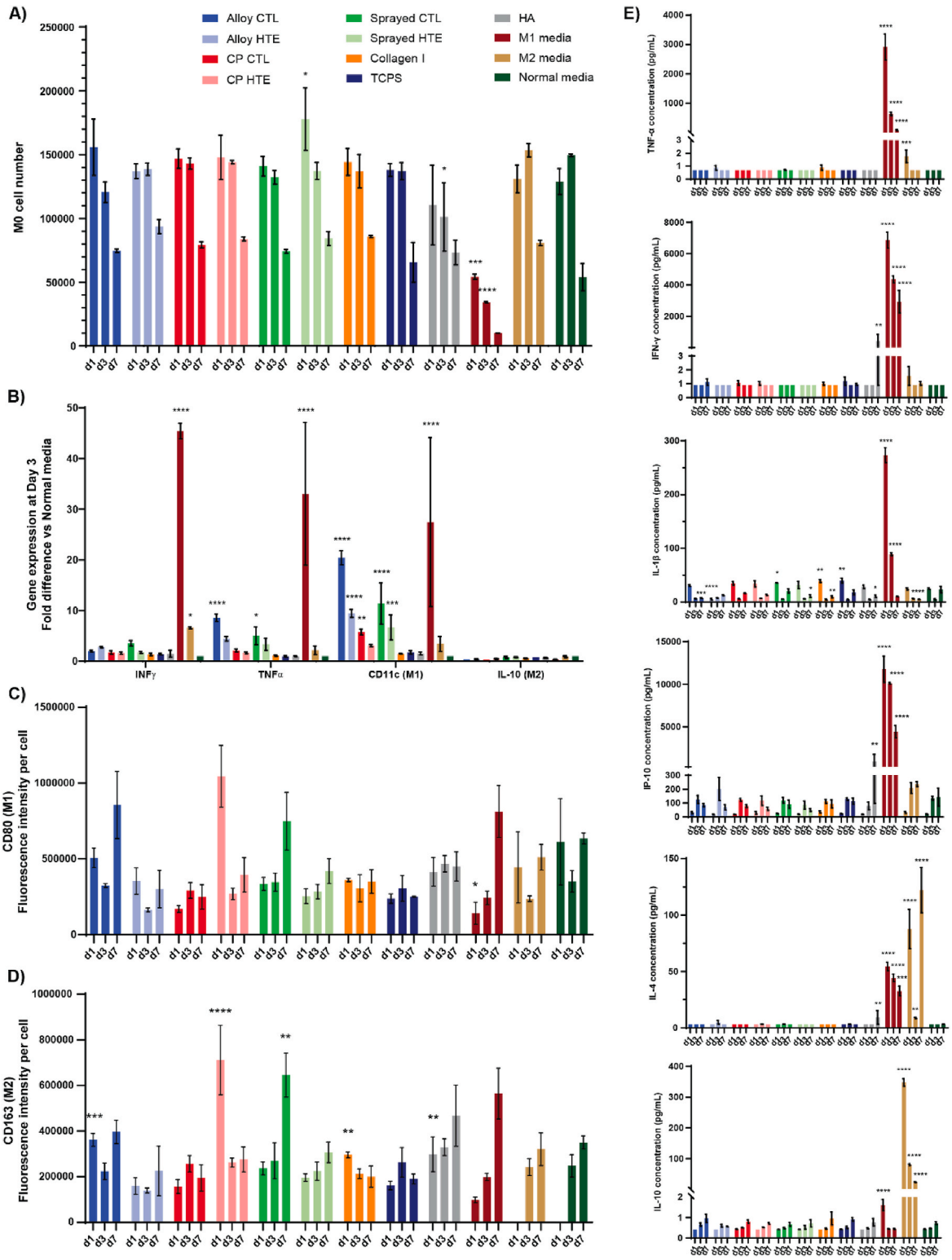


**Fig. 6.** Macrophage differentiation profile upon incubation in 0.7 % supernatant of platelets cultured on the different surfaces, or in control M1, M2, or normal media. A) Cell viability from day 1 to day 7 measured using resazurin ($n = 3$). B) Gene expression of key macrophage differentiation genes at day 3 ($n = 3$), showing fold difference in comparison to normal non-supplemented culture media. C-D) Fluorescence intensity per cell measured from microscopy images ($n = 3$) using ImageJ, following staining for CD80 (M1 marker) and CD163 (M2 marker) respectively. E) Pro-inflammatory and pro-healing cytokines produced by macrophages over time using LegendPlex™ flow cytometry, with TNF-α, IFN-γ, IL-1β and IP-10 associated with pro-inflammatory phenotype, while IL-4 and IL-10 are considered to be more pro-healing factors ($n = 3$). All graphs show mean ± SEM. One-way ANOVA with Dunnett's multiple comparison tests against normal media control (*$p < 0.05$; **$p < 0.01$; ***$p < 0.001$ and ****$p < 0.0001$).

and IP-10, suggesting some level of acute inflammation associated with this material. Levels of secreted IL-1β were initially lower for supernatants from alloy-HTE compared to alloy-CTL and non-supplemented media (5 pg/mL for alloy-HTE vs 30.4 pg/mL for alloy-CTL and 24.9 pg/mL for non-supplemented media on day 1), however, there was no significant difference by day 7. Correlation with gene expression was again variable, highlighting the fact that the low concentrations of platelet supernatant used may have permitted to maintain good cell viability throughout the assay, but perhaps at the expense of more pronounced macrophage polarization. Regarding the pro-healing cytokines, IL-4 and IL-10 secretion was predominantly observed in control M2 media but was essentially identical to the base levels seen in the non-supplemented control media. Overall, when using 0.7 % of platelet supernatant in the cell culture experiments, most macrophages tended to remain at the resting state M0, although some materials (i.e. alloy-CTL and plasma sprayed titania, or HA-coated discs) showed signs of early pro-inflammatory M1 polarization. Most of the materials tested therefore appeared largely inert, which for lack of not encouraging accelerated healing, is at least a testimony to their high biocompatibility towards highly reactive cells such as platelets and macrophages.

Mesenchymal stem cells are multipotent stem cells that play a crucial role in tissue repair, and are predominantly found in the bone marrow. Their ability to differentiate into numerous mesenchymal tissues, including bone (osteoblast), cartilage (chondrocyte) or fat (adipocyte),

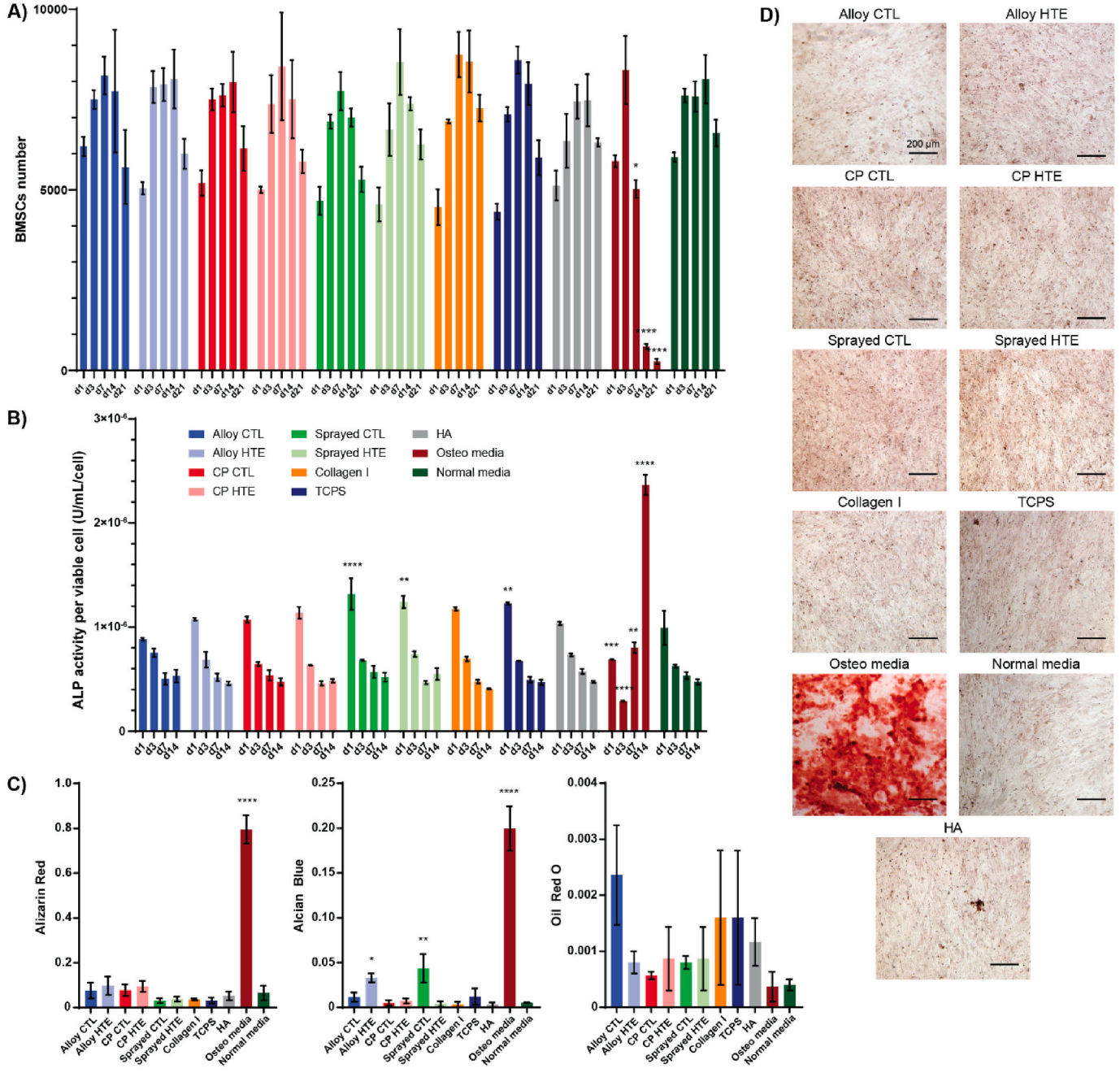


**Fig. 7.** BMSCs differentiation profile upon incubation in 0.7 % v/v supernatant of platelets cultured on the different surfaces, or in control osteoblast and normal media. A) Cell viability from day 1 to day 21 measured using resazurin. B) ALP concentration U/mL/cell. C) Color intensity of BMSCs at day 21 after staining with alizarin red (mineralization indicator), Alcian blue (chondrocyte indicator), or oil red O (adipocyte indicator). D) Representative images of BMSCs stained with alizarin red on day 21. All graphs showing mean ± SEM, $n = 3$. One-way ANOVA with Dunnett's multiple comparison tests against normal media control (*$p < 0.05$; **$p < 0.01$; ***p < 0.001 and ****$p < 0.0001$).

has placed them as one of the main research targets for cell therapy and tissue engineering in the past decades [92,93]. Since improved osseointegration of orthopedic and dental implants is one of the key factors to their long-term integration, preempting the fate of these cells around the implanted site is paramount to our understanding of how well the material will integrate to the surrounding tissues. Platelets and platelet-rich-plasma (PRP) have been shown to facilitate bone healing and remodelling, due to the potent factors being secreted (i.e. TGF-β, PDGF, VEGF or BMP-2) [94,95]. As several of these growth factors were overexpressed by platelets cultured on some of the titanium substrates tested, these surfaces may hold the potential to show an enhanced pro-osseointegration profile. Bone-marrow-derived mesenchymal stem cells (BMSCs) were thus cultured in media supplemented with 0.7 % of platelet supernatant that was collected after 2 h culture on the surfaces, over 21 days. Additional control media were included, with a positive control media known to promote osseointegration "Osteo media" containing 0.1 μM dexamethasone and 10 mM monopotassium phosphate; and a negative control media "Normal media" that wasn't supplemented with platelet supernatant or additional growth factors. Fig. 7A shows the BMSC cell viability in each media throughout the 21-day period. While cell numbers increased from day 1 to day 3 for all the culture media tested, they drastically dropped from day 7 onwards for the control Osteo media (from 8322 cells at day 3, to 5026 at day 7 and 248 at day 21) when they remained stable for the other media tested. This is likely explained by the normal calcification/mineralization process that began to occur in these cells, leading to their apoptosis [96,97]. None of the other media led to changes in viable cell numbers that were significantly different to the ones observed for the normal unsupplemented media. At the concentration tested, the platelet supernatant would therefore appear to have limited effects on the BMSCs cultured. These observations were confirmed by the alkaline phosphatase (ALP) activity measured up to day 14 (Fig. 7B). Considered as one of the most reliable biochemical marker of the early stages of osteogenic differentiation, ALP is known to be secreted by BMSCs as they differentiate into osteoblasts [98,99]. Similarly to what was observed for BMSC viability, all culture media led to comparable results as the normal unsupplemented media with the exception of the osteogenic positive control media. While BMSCs started secreting significantly more ALP from day 7 onwards for the Osteo media, its concentration stayed steady for all other surfaces ($2.4 \times 10^{-6}$ U/mL/cell for the Osteo media on day 14, for around $0.5 \times 10^{-6}$ U/mL/cell for the others, $p < 0.0001$). Interestingly, however, initial ALP levels were significantly higher for both plasma-sprayed surfaces (CTL and HTE) compared to normal media, with $0.99 \times 10^{-6}$ U/mL/cell for the normal media and $1.3 \times 10^{-6}$ U/mL/cell for sprayed-CTL ($p < 0.0001$) and $1.2 \times 10^{-6}$ U/mL/cell for sprayed-HTE ($p = 0.004$). This indicates an early tendency towards osteoblastic differentiation, although that trend didn't appear to continue overtime. Finally, on day 21 the BMSCs were stained to observe whether the BMSCs differentiated into a particular cell lineage, and if so which one. Alizarin red was chosen as a marker for mineralization/osteoblast lineage, Alcian blue was selected as a marker for chondrocyte lineage, and oil red o was used as a marker for adipocyte lineage. At day 21, only the Osteo media showed clear evidence of differentiation towards the osteoblast lineage, with an intense red staining of 0.8 ($p < 0.0001$) being visible for these cells vs around 0.1 for the others (Fig. 7C and **D**). The other surfaces showed no signs of mineralization at that time-point/supernatant concentration. Interestingly, platelet supernatant from alloy-HTE and sprayed-CTL showed a significantly increase in Alcian blue intensity at day 21 compared to normal unsupplemented media: 0.03 for alloy-HTE ($p = 0.04$) and 0,04 for sprayed-CTL ($p = 0.003$), for 0.005 for the normal unsupplemented media. These results indicate that these surfaces may tend to facilitate BMSCs differentiation towards chondrocyte lineage. None of the cell culture media tested appeared to trigger BMSCs differentiation towards the adipocyte lineage.

## 3. Discussion

A wide range of clinically relevant orthopedic materials were selected, namely titanium alloy, commercially pure titanium, and plasma-sprayed titanium, to investigate the consequences of adding antibacterial bioinspired nanostructures in regard to platelet activation. Nanoprotrusions were successfully created onto each material using alkaline hydrothermal etching, with surface properties that were in accordance with the current literature [9–11,13]. Surface nanotopography was identical across all titania, with the nanostructures appearing sharp and randomly-distributed, with a spike height around 400 nm, a width at mid-height of 40–50 nm, and an average spacing between tips of 250 nm. The surface area essentially doubled after the HTE process. Apart from the incorporation of nanostructures into the materials, the hydrothermal etching also led to a thickening of the titanium oxide layer, contributing to the hydrophilicity of the surfaces. Interestingly, the only notable chemical differences between the HTE discs compared to the unetched controls were a) the increase in potassium on the surface due to the use of KOH as the etchant, and b) the crystallinity of the titanium oxide layer. The outermost surface of commercially pure titanium discs indeed retained more potassium than titanium alloy discs, and consisted of a mixture of rutile and anatase phases, while the titanium alloy only displayed crystals in the anatase phase. These differences are likely to impact subsequent cell behavior, either directly, or indirectly by influencing the protein corona forming on the material and with it the subsequent biological interactions. Furthermore, potassium supplementation has been shown to help reduce bone resorption as it may neutralize acid load and thus reduce calcium loss [100,101]. As such, a potassium-enriched interface may also be beneficial to help maintain bone integrity around the implant.

While bioinspired nanostructures have been shown to have impressive antimicrobial properties, there is still little evidence on whether the nanostructures would retain these properties with a protein corona established on the material. Our study showed that all the HTE-Ti surfaces still had substantial bactericidal properties following passivation with human plasma, with the viability of Gram-positive *S. aureus* dropping by 63.5 % and the viability of Gram-negative *P. aeruginosa* consistently dropping by 94.6 %. The nanotopography of the HTE-Ti surfaces appeared to be the leading cause of the antimicrobial properties, with the changes in surface chemistry/presence of a protein corona having little to no effect on the antimicrobial efficacy. These findings are consistent with the "contact-killing" mechanism that has been proposed [59–61].

Platelets are anucleated cell fragments, acting as vigilante of the blood stream integrity, they are extremely sensitive to surface changes. Most surprisingly however, the addition of nanostructures did not have a notable impact on platelet behavior. The number of platelets attaching to the surfaces was inferior or equal to the one seen on TCPS negative control, and the morphologies remained predominantly round. Both of these are indicators of low, if not negligible, platelet activation on the materials tested (either smooth control or HTE-Ti etched). While Kammerer et al. showed that rougher surfaces promoted platelet activation and Hong et al. found that hydrophilic modifications tended to increase thrombogenic responses [27,29], in our study, the HTE-Ti surfaces were shown to be at least as biocompatible as the materials used in patients today. Our findings therefore align with these of both Smith et al. and Yang et al., who showed that titania nanotubes were more blood-compatible than their smooth titanium counterparts [30,31].

Although platelets are similar in size and shape compared to bacteria (0.5–1.5 μm for *S. aureus*, 1–5 μm long and 0.5–1.0 μm wide for *P. aeruginosa*, and 2–3 μm diameter for circulating/non-activated platelets), their interaction with the HTE-Ti surface was radically

different. This is likely explained by the fact that, if their size and shape are similar, the stiffness of their membranes is very different. Platelets are indeed known to be extremely flexible/elastic entities, as they are designed to reach the smallest capillaries. The Young's modulus of platelets has been shown to be around 0.03–0.2 MPa, while it is in the range of 0.5–25 MPa for *S. aureus* and *P. aeruginosa* [102–108]. The viability of bacteria and platelets observed on the nanostructures thus appears directly correlated to the elasticity of the cell wall. Platelets are the most elastic of the 3, while *P. aeruginosa* (Gram-negative) is expected to be more sensitive to stretching than *S. aureus* (Gram-positive) which has a thicker peptidoglycan layer. It has been suggested that cells are more likely to withstand the mechano-bactericidal effect if they are either highly elastic (i.e. they conform to the topography) or highly rigid (i.e. they mostly resist deformation) [11,109]. If a cell can do neither of these, they are more likely to succumb to the hostile effects of the nanostructured topography. This aligns with the observations herein, where the stretch-resistant *S. aureus* and the highly flexible platelet were both more able to withstand mechanical stress compared to the moderately elastic *P. aeruginosa*.

Platelets appeared to survive well on the HTE-Ti surfaces despite the nanostructures, with only a marginal increase in platelet attachment and spreading observed. Interestingly, the concentration in TSP-1 was found to be significantly higher on most substrates compared to the commercial native plasma. Since that factor was shown to associate/serve as an adhesion site for Gram-positive bacteria, thereby facilitating their environment colonization and escape from the immune system, it could be another contributing factor for *S. aureus*'s superior affinity to the titania materials in comparison to *P. aeruginosa* [80,110–112].

In agreement with the microscopy observations of platelets remaining quite inert on the substrates tested, the amount of pro-inflammatory cytokines they released were found to be no different to the one found in commercial native plasma (background levels), meaning that there was no substantial platelet activation on the titanium surfaces (with or without the nanostructures). Titanium alloy was even found to become more biocompatible after the addition of the nanostructures, with fewer platelets attaching to the alloy-HTE than on the smooth control, and less pro-inflammatory factors PF4 and β-TG being secreted. The increased biocompatibility of the alloy-HTE is possibly due to the thickening of the oxide layer and the associated reduced leaching of ions. Indeed, although the use of Ti6Al4V alloy is generally found to be safe and is commonly used in medical devices, there is relevant literature reporting the metallic ion release of aluminium and vanadium, which can have detrimental effects such as interfering with cell viability and proliferation, possibly leading to poor implant integration later on [113–117]. Additionally, the difference in platelet behavior between alloy and commercially pure titania raised the question of the importance of the chemical identify of the surface, given that both surfaces presented the same topography. Most likely, the difference in potassium content of the surface (CP-HTE displaying more potassium than alloy-HTE) and crystallinity (CP-HTE presenting titania in both rutile and anatase phase, while alloy-HTE only showed a large anatase peak) influenced cell behavior via either direct contact or indirectly by leading to small variations in the amount and/or identity of the proteins adhering to the material, subsequently influencing platelets behavior [62,63,118]. In regards to pro-healing factors, commercially pure titania also seemed to display superior abilities compared to the alloy. Platelets indeed secreted more TGF-β and BMP-2 on these surfaces, factors known to respectively: a) mediate wound healing, angiogenesis, ECM formation and immune response and b) be a potent osteogenic factor [119–122]. Interestingly, all titanium-based surfaces tested showed a profile trending more towards a pro-healing outcome, with an increased secretion of PDGF-BB being observed throughout compared to controls, a factor that is known to enhance the proliferation/migration of fibroblasts and general wound healing [123,124].

When looking at the impact of the factors released by platelets upon contact with the materials on key cells associated with inflammation and tissue regeneration, supplementing the culture media with 0.7 % of platelet supernatant (concentration which showed optimal cell viability across several cell types - unpublished results) did not appear to significantly influence their behavior. Both macrophages and BMSCs exhibited similar low to undifferentiated profiles whether in contact with platelets supernatant from HTE-Ti or unetched titania. Albeit no clear cell differentiation could be observed in both cases, none of the HTE-Ti surfaces led to a cell subtype that would be detrimental to the long-term integration of the implant either (i.e. pro-inflammatory M1 polarization for macrophages or adipocyte lineage for the BMSCs). The fact that all surfaces tested remained biologically inert despite the presence of bioactive nanostructures, is a testimony to their potential to be well-accepted by biological environments. The platelet supernatant from HA-coated titanium, also had little to no-impact on cell differentiation compared to non-supplemented culture media. In further studies, perhaps the use of higher percentages of platelet supernatant would be required to mimic the interaction with cells in the direct surroundings of the implant, rather than with cells located further away.

Last but not least, our overall *in vitro* results for HTE-Ti modified titania indicate that the addition of nanostructures outperforms the HA-coated titanium, which is the current gold standard in terms of osseointegration and biocompatibility in the field of orthopedics. Not only were the HA-coated discs associated with the establishment of a dense fibrin layer upon contact with human plasma and a consequently high number of spread platelets attaching to the surface, but these surfaces also led the platelets to secrete more pro-inflammatory factors (i.e. TxB2) and less pro-healing factors (i.e. BMP-2 or PDGF-BB) compared to the other titanium-based surfaces tested. Additionally, HA-coated discs promoted the establishment of a dense biofilm layer which would point to an increased risk of persistent implant infection in patients, whereas the HTE-Ti modified surfaces were associated with efficient bacteria killing.

## 4. Conclusion

This study showed that the bioinspired nanostructures on the HTE-Ti surfaces combined both impressive antibacterial properties in a complex *in vivo*-mimicking environment, and a superior blood biocompatibility profile in terms of platelet activation. Not only the addition of nanostructures did not negatively impact the original biocompatible properties of the titanium, but in the case of titanium alloy in particular, the material became even more blood-compatible. Additionally, direct comparisons with well-established controls and clinically relevant materials throughout the study enabled us to demonstrate the excellent safety profile and biocompatibility of these promising nanoengineered surfaces. Although further *in vivo* studies are required to validate these results, such bioinspired hydrothermally etched surfaces certainly show promise to be safely applied to the surface of biomedical devices such as these used in orthopedics, trauma and dentistry.

## 5. Materials and methods

### 5.1. Surfaces tested and fabrication of the titanium nanostructured surfaces

Discs (10 mm in diameter, 3 mm in height, Supplier: Hamagawa Industrial, Kedah, Malaysia) of titanium alloy Grade 5 Ti6Al4V (henceforth referred to as Alloy), commercially pure (CP) titanium (Grade 2), and commercially pure titanium plasma sprayed onto titanium alloy (henceforth referred to as Sprayed) were hydrothermally treated in a PTFE-lined stainless-steel reactor (Parr Instrument Company, USA), using 1M KOH aqueous solution. The samples made of titanium were further described as "titanium-based" (i.e. Alloy, CP and Sprayed), and the ones that were hydrothermally etched were referred to as "HTE-Ti". Based on preliminary optimization experiments to investigate the generation of distinct nanostructures [125], the reactor

was kept sealed at 150 °C inside an oven for 5 h. After the reaction, the vessels were cooled down in flowing water and the samples were rinsed and immersed in ultrapure water. After drying, discs were heat treated inside a tubular furnace and cooled down overnight until room temperature (RT). As-received titanium discs (CTL), collagen I coated glass coverslips (Collagen I), Thermanox coverslips (TCPS), or hydroxyapatite-coated titanium (HA-Ti) discs were used as control surfaces and hydrothermally treated titanium surfaces (HTE-Ti) were the experimental surfaces. All titanium samples were autoclaved (135 °C, 100 KPa, 12 min), while the other controls were sterilized by 30 min exposition to UVs in a biosafety cabinet.

### 5.2. Surface characterization

*XPS:* Atomic composition within the top 10 nm of the outermost layer was measured using X-ray photoelectron spectroscopy (XPS). XPS survey spectra were collected using a Kratos AXIS Ultra DLD spectrometer (Kratos Analytical Ltd., Manchester, UK) equipped with a magnetically confined charge compensation system, with monochromatic AlK radiation ($h\gamma = 1486.7$ eV). A 300 μm × 700 μm area was analyzed for each substrate ($n = 3$), at a pass energy of 160 eV. Data analysis was performed with CasaXPS software (Casa Software Ltd., Teignmouth, UK). All binding energies were referenced to the aliphatic C1s peak at 285.0 eV.

*AFM:* Atomic Force Microscopy (AFM) images were acquired in ambient using a Bruker Dimension Fastscan AFM contained in an acoustic hood. Amplitude Modulation mode was performed over a 5 × 5 μm and a 20 × 20 μm area of each sample using an NT-MDT NSG30 silicon nitride cantilever with a conical tip rated by the manufacturer at a radius less than 10 nm and a half-side angle of 18°. A spring constant value was derived through a non-contact tuning process, obtaining a spring constant of 36 N/m. A scan velocity of 0.7 Hz optimized cantilever tip surface tracking over the control and high roughness HTE-Ti samples. Plasma-sprayed surfaces were unable to be stably scanned due to high roughness values and adhesion effects.

*Contact Angle:* The wettability of each substrate was measured using the sessile drop method, with a contact angle goniometer model RDSDM02 (RD Support, Edinburgh, UK). 4 μL droplet of ultrapure water was deposited on the substrates, and its silhouette was imaged, and the contact angle measured by a tangent fitting method using plugin Contact_Angle.jar for ImageJ software version 1.53f51 (NIH, Bethesda, MD, USA).

*Spike measurement/SEM:* Scanning electron microscope (SEM) was performed for each substrate, to examine the general topography of these substrates and determine the nanostructures' characteristics. A field emission gun scanning electron microscope Zeiss Merlin FEG-SEM (Zeiss, Germany) equipped with a secondary electron (SE) detector was used, with a 2 kV acceleration potential at 5–50 K times magnification. The sample stage was tilted at 45° to obtain pseudo-side views of the spikes, and was only left orthogonal when measuring the spacing between spikes. The height of the nanostructures was determined by the linear distance between a basal plane and the highest point of each spike, and the width was measured at mid-height in parallel orientation with the basal plane ($n = 180$). A correction factor of x/cos (45°) was applied to account for dimensional distortion from the tilt. The spacing between spikes was determined from non-tilted SEM images ($n = 18$). Spike measurements were made using ImageJ software version 1.53f51 (NIH, Bethesda, MD, USA).

*Grazing angle x-ray diffraction (GAXRD):* The surface crystalline composition of titanium samples was verified on representative discs before and after alkaline heat treatment, using an Empyrean I Grazing angle x-ray diffraction (GAXRD) machine (Malvern Panalytical, United Kingdom) equipped with a Cu K-α detector operated at 45 kV and 40 mA. To generate a crystallinity profile at two different depths from the surface, incident angles of 4°, and 12° were used (penetration of 2 μm and 5 μm respectively), with a 2θ range of 15°–80°. Semi-quantitative analysis was performed using HighScore Plus software (Malvern Panalytical, United Kingdom) for phase identification coupled with peak fitting using the Pawley refinement method to ascertain the composition change with increasing grazing angle and corresponding penetration depth.

### 5.3. Protein pre-conditioning

All surfaces (sterile) were first pre-conditioned with pooled human plasma (#IPLANAC500mL; lot 32653), with overnight incubation at 37 °C under constant gentle agitation on a 3D rocker, in order to more closely mimic the protein corona that would form within seconds on the materials *in vivo*. Surfaces were washed with sterile phosphate-buffered saline (PBS) before use, to remove loosely bound soft corona.

### 5.4. Bacteria study

#### 5.4.1. Bacterial culture and inoculation

*S. aureus* ATCC 25923 and *P. aeruginosa* ATCC 15692 were retrieved from glycerol stocks stored at −80 °C and cultured overnight on tryptone soy agar (TSA) plates. Single colonies of each species were aseptically transferred to 5 mL of tryptone soy broth (TSB) and incubated at 37 °C until the late-log phase. Cell density was then measured by a spectrophotometer (Nanodrop 2000, Thermo Scientific, MA, USA) at 600 nm wavelength. Cell density was adjusted to $10^6$ colony-forming units (CFU)/mL. All surfaces which were pre-conditioned with human serum were inoculated with $10^6$ CFU and incubated for 18 h at 37 °C on an orbital shaker at 90 RPM.

#### 5.4.2. Bacterial viability analysis by live/dead staining

After incubating samples with bacteria, the samples were gently rinsed with PBS to remove non-adherent cells. Samples were then stained with LIVE/DEAD® BacLight™ Bacterial Viability Kit (ThermoFisher Scientific, Waltham, MA, USA) with equal proportions of propidium iodide (PI) and Syto9 at 1.5 μL/mL of PBS, and incubated for 15 min in the dark at room temperature. Next, the samples were inverted onto a glass coverslip and imaged with an Olympus FV3000 confocal laser scanning microscope (CLSM; Olympus, Tokyo, Japan). The excitation and emission spectra were 490/635 for PI and 480/500 nm for Syto9. Triplicate images were taken at random locations for each sample. Live and dead cells were quantified using ImageJ v1.53 (NIH, MD, USA).

### 5.5. Platelet study

#### 5.5.1. Platelet isolation and seeding

30 mL of blood was collected into 3.2 % sodium citrate S-Monovette (Sarstedt #02.1067.001) from three healthy volunteers who gave their written consent (University of South Australia human ethics #202841). A complete blood count (CBC) was performed to evaluate the initial platelet number and verify that blood was within normal acceptable ranges. The blood was then centrifuged at 200 g for 15 min to separate the upper platelet-rich plasma from the other blood components. Platelet concentration was adjusted to 1–3 x $10^7$ platelets/mL (depending on the total number of platelets collected) using sterile PBS, and then seeded onto the surfaces and incubated in sterile 48-well plates for 2 h at 37 °C under constant gentle agitation on a 3D rocker. Platelets from each donor were used in independent experiments.

#### 5.5.2. Supernatant collection

After incubation, the supernatant was collected into sterile low binding 1.5 mL tubes (Eppendorf, Hamburg, Germany) and stored at −80 °C for subsequent enzyme-linked immunosorbent assay (ELISA) assays and cell differentiation in conditioning media experiments.

#### 5.5.3. Platelet fluorescence staining and image analysis

Platelets attached to the surface were fixed with 4 % formaldehyde, then permeabilized with 0.25 % Triton X, before being stained with Phalloidin-TRITC (#ab235138) to allow the visualization of platelet cytoskeleton. Surfaces were imaged at 40× magnification using either a fluorescence microscope (Olympus IX83) for the smooth surfaces, or a confocal microscope (Nikon A1R) for the plasma-sprayed titanium and hydroxyapatite-coated samples. For each donor, triplicates of surfaces were prepared for each condition, and a minimum of 9 images were taken for each surface ($n = 27$). Platelets on each image were manually counted using ImageJ to discriminate between 3 morphologies: spread, dendritic and round.

#### 5.5.4. Scanning electron microscopy (SEM)

Platelets attached to the surface were fixed with 4 % formaldehyde, and then dehydrated using an ethanol gradient. Final dehydration was performed using Critical Point Dryer (CPD). Surfaces were then coated with 10 nm of platinum with a high-resolution sputter coater, to permit visualization of biological entities with the SEM. Surfaces were imaged using a scanning electron microscope (Carl Zeiss Microscopy Crossbeam 540 with GEMINI II column) with an accelerating voltage of 2 kV, a probe current of 100 pA, and a working distance of 3 mm.

#### 5.5.5. Analysis of platelet secreted factors via ELISA or flow cytometry

ELISA or Multiplex assays were performed as per manufacturer instructions, and briefly outlined below. Platelet factor 4 (PF4) and β-TG (CXCL7) Human ELISA assays were performed as per the manufacturer's instruction (#ab189573 and #ab216171 respectively). Standards and solutions were prepared on the day, and samples were incubated for 1 h at RT under constant shaking (300 rpm) to maximize protein binding. Absorbance at 450 nm was measured using a FLUOstart Optima Microplate reader.

Thromboxane B2 (TxB2) ELISA assay was performed as per the manufacturer's instruction (#ab133022). Standards and solutions were prepared on the day, and 10 μL/mL of indomethacin was added to each sample to inhibit prostaglandin synthetase activity. Samples were incubated for 2 h at RT under constant shaking (300 rpm) to maximize protein binding. At the end of the assay, absorbance at 405 nm was measured using a FLUOstar Optima Microplate reader and corrected for 570 nm readings as advised.

Thrombospondin 1 (TSP-1) Human ELISA assay performed as per manufacturer's instruction (#ab193716). Standards and solutions were prepared on the day, and samples were incubated overnight at 4 °C under gentle shaking (25 rpm) to maximize protein binding. At the end of the assay, absorbance at 450 nm was measured using a FLUOstar OPTIMA microplate reader (BMG Labtech, Ortenberg, Germany).

For all the ELISA assays, duplicate readings were obtained for each donor ($n = 6$).

Custom Human Multiplex was performed as per the manufacturer's instruction (BioLegend, CA, USA). Standards and solutions were prepared on the day, and samples were incubated for 2 h at RT under constant shaking (300 rpm) to maximize protein binding. At the end of the assay, samples were read using a BD LSRFortessa™ cell analyzer - flow cytometer (BD Bioscience, CA, USA). Concentrations of human TGF-β, FGF, PDGF-BB, VEGF and BMP-2 were established by converting the Mean Fluorescence Intensity (MFI) value into pg/mL using their respective standard curves as directed by the LEGENDplex™ Data Analysis Software (Version 8). Duplicate readings were obtained for each donor (3), and an assay was performed twice (n = 12).

### 5.6. Macrophage and BMSCs differentiation study

#### 5.6.1. M0 culture and differentiation assay

Monocytes THP-1 (SKU:88081201, Sigma Aldrich, MI, USA) were cultured in RPMI medium (Sigma-Aldrich, MI, USA) supplemented with 10 % Fetal Bovine Serum (FBS, Thermo Fisher Scientific, MA, USA), penicillin/streptomycin and 2 mM Glutamax. Monocytes THP-1 were differentiated into macrophages with 100 ng/mL phorbol 12 myristate 13-acetate (PMA) added into the media for 24 h. Macrophages were seeded at $2 \times 10^5$ cells per well in 48 well plates in PMA-free media and cultured for 24 h. Afterwards, the medium was changed to a conditioned medium containing 0.7 % platelet supernatant and cultured for 7 days. That concentration was selected because preliminary assays showed best cell viability, thus allowing for prolonged culture times (data not shown). LEGENDplex™ Human macrophages/microglia panel (13-plex) kit (BioLegend, CA, USA) was used for the flow cytometry analysis and used as per manufacturer's protocol. Briefly: cell culture supernatant was mixed with assay buffer and mixed beads; and incubated for 2 h at RT under constant shaking (800 rpm). At the end of the assay, samples were read using a BD LSRFortessa™ cell analyzer - flow cytometer (BD Bioscience, CA, USA). For fluorescence staining, the THP-1 cells were fixed in 4 % formaldehyde and permeabilized with 0.2 % Triton for 10 min. The actin filaments were stained with rhodamine-phalloidin (Invitrogen) for 30 min. Macrophages specific markers were stained using Alexa Fluor 488 antibodies anti-human CD80 (BioLegend, CA, USA) and Alexa Fluor 647 anti-human CD163 (BioLegend, CA, USA) and incubated in 1 % BSA-PBS for 1 h. The samples were washed and mounted using the mounting media DAPI Fluoromount G (ProSciTech, QLD, Australia). Samples were imaged using an IX83 Fluorescence Microscope (Olympus, Tokyo, Japan). Fixed exposure time was used to compare fluorescence intensity between different conditions. The fluorescence intensity was analyzed using ImageJ V 1.53 k (NIH, MD, USA).

#### 5.6.2. BMSCs culture and differentiation assay

BMSC were cultured in αMEM medium (Thermo Fisher Scientific, MA, USA) with 10 % FBS, 50 U/mL penicillin, 50 μg/mL streptomycin, 2 mM GlutaMax, 1 mM sodium pyruvate and 100 μM ascorbic acid-2-phosphate. $2 \times 10^4$ BMSC cell/well were seeded in 48 well plates. Cells were cultured over 21 days in a conditioned medium containing 0.7 % platelet supernatant in a humidified incubator at 37 °C and 5 % $CO_2$. That concentration was selected because preliminary assays showed best cell viability, thus allowing for prolonged culture times (data not shown). The synthesis of alkaline phosphatase (ALP) in BMSC was analyzed in media supernatant using Alkaline Phosphatase Assay Colorimetric Kit (Abcam). The analysis was performed according to the manufacturer's protocol. Briefly, samples and PNPP solution were incubated for 1 h at RT protected from light. At the end of the assay, absorbance was measured at 405 nm.

The following staining was performed to evaluate BMSC differentiation:

- *Mineralization*: Cells were fixed in 4 % formaldehyde for 15 min. 2 % Alizarin Red S (Chem-Supply, SA, Australia) was prepared in water and the pH was adjusted to 4.1 using 0.5 % ammonium hydroxide (Sigma-Aldrich, MI, USA). BMSCs were incubated in alizarin solution for 20 min at RT and washed with water 3 times to remove unbound dye.
- *Chondrogenesis*: Alcian blue at pH 2.5 in 3 % acetic acid (Sigma-Aldrich, MI, USA) was added as supplied, incubated for 15 min, and washed thoroughly in water.
- *Adipogenesis*: BMSCs were incubated with propylene glycol for 5 min, then in Oil Red O (Abcam, Cambridge, UK), heated (60 °C) for 10 min and differentiated in 85 % propylene glycol for 1 min. Samples were washed in water and incubated in hematoxylin for 2 min and again washed thoroughly in water.

Three random images were acquired from each sample, with fixed exposure time at magnification 20×. Color intensity was then analyzed using Image J and the plugins for the calculation of the intensity of red, blue, and purple.

#### 5.6.3. THP-1 and BMSC viability

The 150 μg/mL resazurin sodium salt (Sigma-Aldrich, MI, USA) stock solution in Milli-Q water was filtered using a 0.2 μm filter and stored in a light-protected container at 4 °C. Resazurin was added into fresh media (25 μg/mL), incubated for 4 h and read using a microplate reader. The fluorescence was analyzed with excitation at 540 nm and emission at 590 nm.

#### 5.6.4. Gene expression of M0 and BMSCs on day 3

RNA was extracted using RiboPure™ Kit (Life Technologies, CA, USA) according to the manufacturer's instructions. Briefly, cells were homogenized using Tri Reagent for 5 min at RT and centrifuged at 12000 g for 10 min at 4 °C. RNA was extracted with chloroform. The samples were vortexed for 15 s, incubated for 5 min at RT, and centrifuged. 400 μL of the aqueous phase was moved to a new tube and purified with 100 % ethanol and a filter cartridge. The RNA was eluted with elution buffer and centrifuged for 30 s. RNA was stored at −80 °C until required for PCR analysis. The reverse transcription PCR was performed using SuperScript® III Platinum® SYBR® Green One-Step qRT-PCR Kit (Invitrogen, MA, USA) according to manufacturer protocol. Briefly, Master Mix was prepared using 1 μl SuperScript, 25 μl SYBR Green, 1 μl forward primer, 1 μl reverse primer, and DEPC-water for a final volume of 50 μl including template. The PCR reaction was run using CFX connect real-time PCR detection system (Bio-Rad, CA, USA) with the standard reaction parameters: 50 °C 3 min, 95 °C 5min, 40 cycles of 95 °C 15 s, 60 °C 30 s, 40 °C 1min. All primers were synthesised by Invitrogen (MA, USA), apart from IL-10 which was provided by Applied Biosystems (TaqMan Gene Expression Assay Hs00961622_m1). The primer sequences are shown below.

| | Forward Primer Sequence | Reverse Primer Sequence |
|---|---|---|
| GADPH | 5′-TGACGCTGGGGCTGGCATTG-3′ | 5′-GCTCTTGCTGGGGCTGGTGG-3′ |
| CD11c | 5′-ACTTCACGGCCTCTCTTCC-3′ | 5′-CACCAGGGTCTTCAAGTCTG-3′ |
| TNF-α | 5′-TGCTCCTCACCCACACCAT-3′ | 5′-GGAGGTTGACCTTGGTCTGGTA-3′ |
| INF-γ | 5′-CTAATTATTCGGTAACTGACTTGA-3′ | 5′-CTAATTATTCGGTAACTGACTTGA-3′ |

### 5.7. Statistical analysis

One-way ANOVA with Tukey's multiple comparison tests was used to statistically analyze bacteria and platelet counts using GraphPad with GraphPad Prism version 9 for Windows (GraphPad Software, La Jolla CA, USA, www.graphpad.com). While one-way ANOVA with Dunnett's multiple comparison tests against Commercial Native Plasma control or Normal media control was used to analyze ELISA/Multiplex platelet readings or macrophage and BMSC readings respectively. A $p$-value of $<0.05$ was considered significant for all tests. $^{*}p < 0.05$; $^{**}p < 0.01$; $^{***}p < 0.001$; $^{****}p < 0.0001$.

## CRediT authorship contribution statement

**Anouck L.S. Burzava:** Writing – review & editing, Writing – original draft, Visualization, Validation, Supervision, Project administration, Methodology, Investigation, Formal analysis, Conceptualization. **Agnieszka Zuber:** Writing – review & editing, Investigation. **Andrew Hayles:** Writing – review & editing, Investigation. **James Morel:** Writing – review & editing, Visualization, Investigation, Formal analysis. **Richard Bright:** Writing – review & editing. **Jonathan Wood:** Writing – review & editing, Investigation. **Dennis Palms:** Writing – review & editing, Resources. **Dan Barker:** Writing – review & editing, Resources, Project administration, Funding acquisition, Conceptualization. **Toby Brown:** Writing – review & editing, Validation, Supervision, Resources, Project administration, Funding acquisition, Conceptualization. **Krasimir Vasilev:** Writing – review & editing, Supervision, Project administration, Funding acquisition, Conceptualization.

## Declaration of competing interest

The authors declare the following financial interests/personal relationships which may be considered as potential competing interests: All authors reports financial support and equipment, drugs, or supplies were provided by Corin Australia Pty Ltd. All authors reports financial support was provided by Innovative Manufacturing Cooperative Research Centre. All authors reports financial support was provided by Global Orthopaedic Technology Pty Ltd. Dan Barker and Toby Brown has patent #EP3041787B1 - A synthetic biocidal surface comprising an array of nanospikes issued to Global Orthopaedic Technology Pty Ltd. If there are other authors, they declare that they have no known competing financial interests or personal relationships that could have appeared to influence the work reported in this paper.

## Data availability

Data will be made available on request.

## Acknowledgements

This study was co-funded by the Department of Industry, Science, Energy and Resources (Innovative Manufacturing CRC Ltd) Global Orthopaedic Technology Pty Ltd (IMCRC/GOT/130318). The authors acknowledge the funding and in-kind support from Corin Australia and the University of South Australia. The authors would also like to acknowledge the instruments and technical assistance of Microscopy Australia at the University of South Australia Mawson Lakes Campus, a facility that is funded by the University, and State and Federal Governments, as well as the use of facilities in the Solid State & Elemental Analysis Unit at Mark Wainwright Analytical Centre, UNSW Sydney. They would also like to thank Clinpath Pathology Australia, in particular, Izabela, for their assistance with the blood collection. KV thanks NHMRC for Fellowship GNT1194466 and ARC for grant DP180101254.

## Appendix A. Supplementary data

Supplementary data to this article can be found online at https://doi.org/10.1016/j.mtbio.2024.101236.

## References

[1] U. Desa, World population prospects 2019: highlights, New York (US): United Nations Department for Economic and Social Affairs 11 (1) (2019) 125.
[2] Fortune-business-insights orthopedic implants market size, share & COVID-19 impact analysis - forecast 2022-2029. https://www.fortunebusinessinsights.com/industry-reports/orthopedic-implants-market-101659. (Accessed 18 August 2022).
[3] S. Kurtz, K. Ong, E. Lau, F. Mowat, M. Halpern, Projections of primary and revision hip and knee arthroplasty in the United States from 2005 to 2030, Jbjs 89 (4) (2007) 780–785.
[4] C. Stewart, B. Akhavan, S.G. Wise, M.M. Bilek, A review of biomimetic surface functionalization for bone-integrating orthopedic implants: mechanisms, current approaches, and future directions, Prog. Mater. Sci. 106 (2019) 100588.
[5] C. Mas-Moruno, B. Su, M. Dalby, Multifunctional coatings and nanotopographies: toward cell instructive and antibacterial implants, Adv. Healthcare Mater. 8 (2019).
[6] E.J. Tobin, Recent coating developments for combination devices in orthopedic and dental applications: a literature review, Adv. Drug Deliv. Rev. 112 (2017) 88–100.
[7] Q. Hong, B.e. Nie, Special issue: multifunctional coatings in orthopedic implants, Coatings 12 (7) (2022) 967.
[8] E.P. Ivanova, J. Hasan, H.K. Webb, V.K. Truong, G.S. Watson, J.A. Watson, V. A. Baulin, S. Pogodin, J.Y. Wang, M.J. Tobin, C. Löbbe, R.J. Crawford, Natural bactericidal surfaces: mechanical rupture of Pseudomonas aeruginosa cells by Cicada wings, Small 8 (16) (2012) 2489–2494.
[9] E.P. Ivanova, J. Hasan, H.K. Webb, G. Gervinskas, S. Juodkazis, V.K. Truong, A. H. Wu, R.N. Lamb, V.A. Baulin, G.S. Watson, Bactericidal activity of black silicon, Nat. Commun. 4 (1) (2013) 1–7.

[10] C.M. Bhadra, V. Khanh Truong, V.T. Pham, M. Al Kobaisi, G. Seniutinas, J. Y. Wang, S. Juodkazis, R.J. Crawford, E.P. Ivanova, Antibacterial titanium nano-patterned arrays inspired by dragonfly wings, Sci. Rep. 5 (1) (2015) 1–12.
[11] A. Hayles, J. Hasan, R. Bright, D. Palms, T. Brown, D. Barker, K. Vasilev, Hydrothermally etched titanium: a review on a promising mechano-bactericidal surface for implant applications, Mater. Today Chem. 22 (2021) 100622.
[12] R. Bright, D. Fernandes, J. Wood, D. Palms, A. Burzava, N. Ninan, T. Brown, D. Barker, K. Vasilev, Long-term antibacterial properties of a nanostructured titanium alloy surface: an in vitro study, Materials Today Bio 13 (2022) 100176.
[13] R. Bright, A. Hayles, J. Wood, N. Ninan, D. Palms, R.M. Visalakshan, A. Burzava, T. Brown, D. Barker, K. Vasilev, Bio-inspired nanostructured Ti-6Al-4V alloy: the role of two alkaline etchants and the hydrothermal processing duration on antibacterial activity, Nanomaterials 12 (7) (2022) 1140.
[14] C.F. Jones, R.D. Quarrington, H. Tsangari, Y. Starczak, A. Mulaibrahimovic, A.L. S. Burzava, C. Christou, A.J. Barker, J. Morel, R. Bright, D. Barker, T. Brown, K. Vasilev, P.H. Anderson, A novel nanostructured surface on titanium implants increases osseointegration in a sheep model, Clin. Orthop. Relat. Res. 480 (11) (2022) 2232–2250.
[15] International Organization for Standardization, Biological Evaluation of Medical Devices - Part 22: Guidance on nanomaterials_(ISO/TR 10993-22:2017), 2017.
[16] International Organization for Standardization, Biological Evaluation of Medical Devices - Part 4: Selection of Tests for Interactions with blood_(ISO10993-4: 2017), 2017.
[17] G. Born, P. Richardson, Activation time of blood platelets, J. Membr. Biol. 57 (2) (1980) 87–90.
[18] Y. Hou, N. Carrim, Y. Wang, R.C. Gallant, A. Marshall, H. Ni, Platelets in hemostasis and thrombosis: novel mechanisms of fibrinogen-independent platelet aggregation and fibronectin-mediated protein wave of hemostasis, J Biomed Res 29 (6) (2015) 437–444.
[19] S. Kamath, A. Blann, G. Lip, Platelet activation: assessment and quantification, Eur. Heart J. 22 (17) (2001) 1561–1571.
[20] J.P. Allain, M. Echeverry-Rendón, Surface treatment of metallic biomaterials in contact with blood to enhance hemocompatibility, in: Hemocompatibility of Biomaterials for Clinical Applications, Elsevier, 2018, pp. 279–326.
[21] K.R. Fernandes, Y. Zhang, A.M.P. Magri, A.C.M. Renno, J.J.J.P. van den Beucken, Biomaterial property effects on platelets and macrophages: an in vitro study, ACS Biomater. Sci. Eng. 3 (12) (2017) 3318–3327.
[22] V. Milleret, S. Tugulu, F. Schlottig, H. Hall, Alkali treatment of microrough titanium surfaces affects macrophage/monocyte adhesion, platelet activation and architecture of blood clot formation, Eur. Cell. Mater. 21 (2011) 430–444.
[23] H.T. Shiu, B. Goss, C. Lutton, R. Crawford, Y. Xiao, Controlling whole blood activation and resultant clot properties by carboxyl and alkyl functional groups on material surfaces: a possible therapeutic approach for enhancing bone healing, J. Mater. Chem. B 2 (20) (2014) 3009–3021.
[24] S.A. Skoog, Q. Lu, R.A. Malinauskas, A.V. Sumant, J. Zheng, P.L. Goering, R. J. Narayan, B.J. Casey, Effects of nanotopography on the in vitro hemocompatibility of nanocrystalline diamond coatings, J. Biomed. Mater. Res. 105 (1) (2017) 253–264.
[25] C. Sperling, M. Fischer, M.F. Maitz, C. Werner, Blood coagulation on biomaterials requires the combination of distinct activation processes, Biomaterials 30 (27) (2009) 4447–4456.
[26] M. Xi, Y. Zhang, L. Long, X. Li, Controllable hydrothermal synthesis of rutile TiO2 hollow nanorod arrays on TiCl4 pretreated Ti foil for DSSC application, J. Solid State Chem. 219 (2014) 118–126.
[27] P.W. Kammerer, M. Gabriel, B. Al-Nawas, T. Scholz, C.M. Kirchmaier, M.O. Klein, Early implant healing: promotion of platelet activation and cytokine release by topographical, chemical and biomimetically titanium surface modifications in vitro, Clin. Oral Implants Res. 23 (4) (2012) 504–510.
[28] L. Zhang, X.H. Liao, A. Fok, C.Y. Ning, P. Ng, Y. Wang, Effect of crystalline phase changes in titania (TiO2) nanotube coatings on platelet adhesion and activation, Mat Sci Eng C-Mater 82 (2018) 91–101.
[29] J. Hong, S. Kurt, A. Thor, A hydrophilic dental implant surface exhibit thrombogenic properties in vitro, Clin. Implant Dent. Relat. Res. 15 (1) (2013) 105–112.
[30] B.S. Smith, P. Capellato, S. Kelley, M. Gonzalez-Juarrero, K.C. Popat, Reduced in vitro immune response on titania nanotube arrays compared to titanium surface, Biomater. Sci. 1 (3) (2013) 322–332.
[31] Y. Yang, Y. Lai, Q. Zhang, K. Wu, L. Zhang, C. Lin, P. Tang, A novel electrochemical strategy for improving blood compatibility of titanium-based biomaterials, Colloids Surf. B Biointerfaces 79 (1) (2010) 309–313.
[32] J.R. Lieberman, A. Daluiski, T.A. Einhorn, The role of growth factors in the repair of bone - biology and clinical applications, J Bone Joint Surg Am 84a (6) (2002) 1032–1044.
[33] K. Hu, B.R. Olsen, The roles of vascular endothelial growth factor in bone repair and regeneration, Bone 91 (2016) 30–38.
[34] C.Y. Hu, T.-R. Yoon, Recent updates for biomaterials used in total hip arthroplasty, Biomater. Res. 22 (2018) 33–35.
[35] W.C. Head, D.J. Bauk, R.H. Emerson, Titanium as the material of choice for cementless femoral components in total hip arthroplasty, Clin. Orthop. Relat. Res. 311 (1995) 85–90.
[36] L. Le Guéhennec, A. Soueidan, P. Layrolle, Y. Amouriq, Surface treatments of titanium dental implants for rapid osseointegration, Dent. Mater. 23 (7) (2007) 844–854.
[37] D. Buser, R.K. Schenk, S. Steinemann, J.P. Fiorellini, C.H. Fox, H. Stich, Influence of surface characteristics on bone integration of titanium implants. A histomorphometric study in miniature pigs, J. Biomed. Mater. Res. 25 (7) (1991) 889–902.
[38] J.L. Ong, D.L. Carnes, K. Bessho, Evaluation of titanium plasma-sprayed and plasma-sprayed hydroxyapatite implants in vivo, Biomaterials 25 (19) (2004) 4601–4606.
[39] D.C.R. Hardy, P. Frayssinet, P.E. Delince, Osteointegration of hydroxyapatite-coated stems of femoral prostheses, Eur. J. Orthop. Surg. Traumatol. 9 (2) (1999) 75–81.
[40] L. Sun, C.C. Berndt, K.A. Gross, A. Kucuk, Material fundamentals and clinical performance of plasma-sprayed hydroxyapatite coatings: a review, J. Biomed. Mater. Res. 58 (5) (2001) 570–592.
[41] I. Landor, P. Vavrik, A. Sosna, D. Jahoda, H. Hahn, M. Daniel, Hydroxyapatite porous coating and the osteointegration of the total hip replacement, Arch. Orthop. Trauma Surg. 127 (2) (2007) 81–89.
[42] Z.Y. Yuan, X.B. Zhang, B.L. Su, Moderate hydrothermal synthesis of potassium titanate nanowires, Appl. Phys. A 78 (7) (2004) 1063–1066.
[43] M. Iafisco, M. Marchetti, J. Gómez Morales, M.A. Hernández-Hernández, J. M. García Ruiz, N. Roveri, Silica gel template for calcium phosphates crystallization, Cryst. Growth Des. 9 (11) (2009) 4912–4921.
[44] M.M. Pereira, L.L. Hench, Mechanisms of hydroxyapatite formation on porous gel-silica substrates, J. Sol. Gel Sci. Technol. 7 (1) (1996) 59–68.
[45] N. Sharifi, M. Pugh, C. Moreau, A. Dolatabadi, Developing hydrophobic and superhydrophobic TiO2 coatings by plasma spraying, Surf. Coating. Technol. 289 (2016) 29–36.
[46] R. Bansal, J.K. Singh, V. Singh, D.D.N. Singh, P. Das, Optimization of oxidation temperature for commercially pure titanium to achieve improved corrosion resistance, J. Mater. Eng. Perform. 26 (3) (2017) 969–977.
[47] D.M. Brunette, P. Tengvall, J. Textor, P. Thomsen, Titanium in Medicine: Material Science, Surface Science, Engineering, Biological Responses and Medical Applications, Springer, Zurich, Switzerland, 2001, p. 1029.
[48] C. Sittig, M. Textor, N.D. Spencer, M. Wieland, P.H. Vallotton, Surface characterization of implant materials c.p. Ti, Ti-6Al-7Nb and Ti-6Al-4V with different pretreatments, J. Mater. Sci. Mater. Med. 10 (1999) 35–46.
[49] J. Barberi, S. Spriano, Titanium and protein adsorption: an overview of mechanisms and effects of surface features, Materials 14 (7) (2021) 1590.
[50] D. Baimanov, R. Cai, C. Chen, Understanding the chemical nature of nanoparticle–protein interactions, Bioconjugate Chem. 30 (7) (2019) 1923–1937.
[51] J. Simon, G. Kuhn, M. Fichter, S. Gehring, K. Landfester, V. Mailänder, Unraveling the in vivo protein corona, Cells 10 (1) (2021) 132.
[52] S. Tenzer, D. Docter, J. Kuharev, A. Musyanovych, V. Fetz, R. Hecht, F. Schlenk, D. Fischer, K. Kiouptsi, C. Reinhardt, Rapid formation of plasma protein corona critically affects nanoparticle pathophysiology, Nat. Nanotechnol. 8 (10) (2013) 772–781.
[53] M.P. Monopoli, C. Åberg, A. Salvati, K.A. Dawson, Biomolecular coronas provide the biological identity of nanosized materials, Nat. Nanotechnol. 7 (12) (2012) 779–786.
[54] A. Hayles, J. Hasan, R. Bright, J. Wood, D. Palms, P. Zilm, D. Barker, K. Vasilev, Spiked titanium nanostructures that inhibit anaerobic dental pathogens, ACS Appl. Nano Mater. 5 (9) (2022) 12051–12062.
[55] A. Hayles, R. Bright, J. Wood, D. Palms, P. Zilm, T. Brown, D. Barker, K. Vasilev, Spiked nanostructures disrupt fungal biofilm and impart increased sensitivity to antifungal treatment, Adv. Mater. Interfac. 9 (12) (2022) 2102353.
[56] R. Bright, A. Hayles, J. Wood, D. Palms, T. Brown, D. Barker, K. Vasilev, Surfaces containing sharp nanostructures enhance antibiotic efficacy, Nano Lett 22 (16) (2022) 6724–6731.
[57] V.S. Kattimani, S. Kondaka, K.P. Lingamaneni, Hydroxyapatite—Past, present, and future in bone regeneration, Bone Tissue Regen. Insights 7 (BTRI) (2016) S36138.
[58] U. Ripamonti, L.C. Roden, L.F. Renton, Osteoinductive hydroxyapatite-coated titanium implants, Biomaterials 33 (15) (2012) 3813–3823.
[59] D.P. Linklater, V.A. Baulin, S. Juodkazis, R.J. Crawford, P. Stoodley, E.P. Ivanova, Mechano-bactericidal actions of nanostructured surfaces, Nat. Rev. Microbiol. 19 (1) (2021) 8–22.
[60] J. Jenkins, J. Mantell, C. Neal, A. Gholinia, P. Verkade, A.H. Nobbs, B. Su, Antibacterial effects of nanopillar surfaces are mediated by cell impedance, penetration and induction of oxidative stress, Nat. Commun. 11 (1) (2020) 1–14.
[61] V. Nandakumar, S. Chittaranjan, V.M. Kurian, M. Doble, Characteristics of bacterial biofilm associated with implant material in clinical practice, Polym. J. 45 (2) (2013) 137–152.
[62] M.F. Maitz, M.-T. Pham, E. Wieser, I. Tsyganov, Blood compatibility of titanium oxides with various crystal structure and element doping, J. Biomater. Appl. 17 (4) (2003) 303–319.
[63] Q. Huang, Y. Yang, D. Zheng, R. Song, Y. Zhang, P. Jiang, E.A. Vogler, C. Lin, Effect of construction of TiO2 nanotubes on platelet behaviors: structure-property relationships, Acta Biomater. 51 (2017) 505–512.
[64] E.P. Brass, W.B. Forman, R.V. Edwards, O. Lindan, Fibrin formation: effect of calcium ions, Blood 52 (4) (1978) 654–658.
[65] P.H. Kopper, Role of calcium in fibrin formation, Nature 198 (4879) (1963) 493–494.
[66] S.A. Smith, J.H. Morrissey, Polyphosphate enhances fibrin clot structure, Blood 112 (7) (2008) 2810–2816.
[67] B.-S. Kim, J. Lee, Enhanced bone healing by improved fibrin-clot formation via fibrinogen adsorption on biphasic calcium phosphate granules, Clin. Oral Implants Res. 26 (10) (2015) 1203–1210.
[68] Z.M. Ruggeri, G.L. Mendolicchio, Adhesion mechanisms in platelet function, Circ. Res. 100 (12) (2007) 1673–1685.

[69] B. Savage, E. Saldívar, Z.M. Ruggeri, Initiation of Platelet Adhesion by Arrest onto Fibrinogen or Translocation on von Willebrand Factor, Cell 84 (2) (1996) 289–297.
[70] M. Nakamura, H. Aizawa, H. Kawabata, A. Sato, T. Watanabe, K. Isobe, Y. Kitamura, T. Tanaka, T.A.-O.X. Kawase, Platelet Adhesion on Commercially Pure Titanium Plates in Vitro III: Effects of Calcium Phosphate-Blasting on Titanium Plate Biocompatibility, 2024, pp. 2198–4034.
[71] H. Heijnen, P. van der Sluijs, Platelet secretory behaviour: as diverse as the granules or not? J. Thromb. Haemostasis 13 (12) (2015) 2141–2151.
[72] Y. Chen, H. Zhong, Y. Zhao, X. Luo, W. Gao, Role of platelet biomarkers in inflammatory response, Biomark. Res. 8 (1) (2020) 28.
[73] Z. Li, M.K. Delaney, K.A. O'Brien, X. Du, Signaling during platelet adhesion and activation, Arterioscler. Thromb. Vasc. Biol. 30 (12) (2010) 2341–2349.
[74] S.-H. Yun, E.-H. Sim, R.-Y. Goh, J.-I. Park, J.-Y. Han, Platelet activation: the mechanisms and potential biomarkers, BioMed Res. Int. 2016 (2016) 9060143.
[75] D.W. Thomas, P.N. Rocha, C. Nataraj, L.A. Robinson, R.F. Spurney, B.H. Koller, T. M. Coffman, Proinflammatory actions of thromboxane receptors to enhance cellular immune responses, J. Immunol. 171 (12) (2003) 6389–6395.
[76] C. Patrono, B. Rocca, Measurement of thromboxane biosynthesis in health and disease, Front. Pharmacol. 10 (2019).
[77] D.W. Thomas, C. Rocha Pn Fau - Nataraj, L.A. Nataraj C Fau - Robinson, R. F. Robinson La Fau - Spurney, B.H. Spurney Rf Fau - Koller, T.M. Koller Bh Fau - Coffman, T.M. Coffman, Proinflammatory Actions of Thromboxane Receptors to Enhance Cellular Immune Responses, 2024, pp. 22–1767.
[78] P. Starlinger, Thrombospondin-1: a unique marker to identify in vitro platelet activation when monitoring in vivo processes, J. Thromb. Haemostasis 8 (8) (2010) 1809–1819.
[79] C.-W. Hsu, K. Yuan, C.-C. Tseng, The negative effect of platelet-rich plasma on the growth of human cells is associated with secreted thrombospondin-1, Oral Surg. Oral Med. Oral Pathol. Oral Radiol. Endod. 107 (2) (2009) 185–192.
[80] U. Binsker, T.P. Kohler, S. Hammerschmidt, Contribution of human thrombospondin-1 to the pathogenesis of gram-positive bacteria, J. Innate Immun. 11 (4) (2019) 303–315.
[81] E.M. Golebiewska, A.W. Poole, Platelet secretion: from haemostasis to wound healing and beyond, Blood Rev. 29 (3) (2015) 153–162.
[82] F. Scopelliti, C. Cattani, V. Dimartino, C. Mirisola, A. Cavani, Platelet derivatives and the immunomodulation of wound healing, International journal of molecular sciences 23 (15) (2022) 8370.
[83] F.C. Richter, I. Udalova, Macrophage commonalities across tissues and inflammation, Nat. Rev. Immunol. 22 (1) (2022) 2–4.
[84] M.E. Ogle, C.E. Segar, S. Sridhar, E.A. Botchwey, Monocytes and macrophages in tissue repair: implications for immunoregenerative biomaterial design, Exp. Biol. Med. 241 (10) (2016) 1084–1097.
[85] H.-C. Yang, H.C. Park, H. Quan, Y. Kim, Immunomodulation of biomaterials by controlling macrophage polarization, in: I. Noh (Ed.), Biomimetic Medical Materials: from Nanotechnology to 3D Bioprinting, Springer Singapore, Singapore, 2018, pp. 197–206.
[86] H.T. Idriss, J.H. Naismith, TNF alpha and the TNF receptor superfamily: structure-function relationship(s), Microsc. Res. Tech. 50 (3) (2000) 184–195.
[87] S. Gessani, F. Belardelli, IFN-γ expression in macrophages and its possible biological significance, Cytokine Growth Factor Rev. 9 (2) (1998) 117–123.
[88] C.N. Lumeng, J.B. DelProposto, D.J. Westcott, A.R. Saltiel, Phenotypic switching of adipose tissue macrophages with obesity is generated by spatiotemporal differences in macrophage subtypes, Diabetes 57 (12) (2008) 3239–3246.
[89] F.A. Verreck, T. de Boer, D.M. Langenberg, M.A. Hoeve, M. Kramer, E. Vaisberg, R. Kastelein, A. Kolk, R. de Waal-Malefyt, T.H. Ottenhoff, Human IL-23-producing type 1 macrophages promote but IL-10-producing type 2 macrophages subvert immunity to (myco) bacteria, Proc. Natl. Acad. Sci. USA 101 (13) (2004) 4560–4565.
[90] A. Mantovani, A. Sica, S. Sozzani, P. Allavena, A. Vecchi, M. Locati, The chemokine system in diverse forms of macrophage activation and polarization, Trends Immunol. 25 (12) (2004) 677–686.
[91] E.A. Ross, A. Devitt, J.R. Johnson, Macrophages: the good, the bad, and the gluttony, Front. Immunol. 12 (2021).
[92] A.I. Caplan, Mesenchymal stem cells, J. Orthop. Res. 9 (5) (1991) 641–650.
[93] A. Uccelli, L. Moretta, V. Pistoia, Mesenchymal stem cells in health and disease, Nat. Rev. Immunol. 8 (9) (2008) 726–736.
[94] G. Fernandes, S. Yang, Application of platelet-rich plasma with stem cells in bone and periodontal tissue engineering, Bone Research 4 (1) (2016) 16036.
[95] K. Arvidson, B.M. Abdallah, L.A. Applegate, N. Baldini, E. Cenni, E. Gomez-Barrena, D. Granchi, M. Kassem, Y.T. Konttinen, K. Mustafa, D.P. Pioletti, T. Sillat, A. Finne-Wistrand, Bone regeneration and stem cells, J. Cell Mol. Med. 15 (4) (2011) 718–746.
[96] K.M. Kim, Apoptosis and calcification, Scanning Microsc. 9 (4) (1995) 19.
[97] H. Fujita, M. Yamamoto, T. Ogino, H. Kobuchi, N. Ohmoto, E. Aoyama, T. Oka, T. Nakanishi, K. Inoue, J. Sasaki, Necrotic and apoptotic cells serve as nuclei for calcification on osteoblastic differentiation of human mesenchymal stem cells in vitro, Cell Biochem. Funct. 32 (1) (2014) 77–86.
[98] M. Capulli, R. Paone, N. Rucci, Osteoblast and osteocyte: games without frontiers, Arch. Biochem. Biophys. 561 (2014) 3–12.
[99] A. Sabokbar, P. Millett, B. Myer, N. Rushton, A rapid, quantitative assay for measuring alkaline phosphatase activity in osteoblastic cells in vitro, Bone Miner. 27 (1) (1994) 57–67.
[100] C.M. Weaver, Potassium and health, Adv. Nutr. 4 (3) (2013) 368S–377S.
[101] A. Sebastian, S.T. Harris, J.H. Ottaway, K.M. Todd, R.C. Morris Jr, Improved mineral balance and skeletal metabolism in postmenopausal women treated with potassium bicarbonate, N. Engl. J. Med. 330 (25) (1994) 1776–1781.
[102] S. Sorrentino, J.-D. Studt, M.B. Horev, O. Medalia, K.T. Sapra, Toward correlating structure and mechanics of platelets, Cell Adhes. Migrat. 10 (5) (2016) 568–575.
[103] C. Formosa-Dague, P. Speziale, J. Foster Timothy, A. Geoghegan Joan, F. Dufrêne Yves, Zinc-dependent mechanical properties of Staphylococcus aureus biofilm-forming surface protein SasG, Proc. Natl. Acad. Sci. USA 113 (2) (2016) 410–415.
[104] R. Boudjemaa, K. Steenkeste, A. Canette, R. Briandet, M.-P. Fontaine-Aupart, C. Marlière, Direct observation of the cell-wall remodeling in adhering Staphylococcus aureus 27217: an AFM study supported by SEM and TEM, The Cell Surface 5 (2019) 100018.
[105] R. Trivedi Rishi, A. Crooks John, K. Auer George, J. Pendry, P. Foik Ilona, A. Siryaporn, L. Abbott Nicholas, Z. Gitai, B. Weibel Douglas, V. Gordon, M. Whiteley, Mechanical genomic studies reveal the role of d-alanine metabolism in Pseudomonas aeruginosa cell stiffness, mBio 9 (5) (2024) e01340.
[106] H.H. Tuson, G.K. Auer, L.D. Renner, M. Hasebe, C. Tropini, M. Salick, W.C. Crone, A. Gopinathan, K.C. Huang, D.B. Weibel, Measuring the stiffness of bacterial cells from growth rates in hydrogels of tunable elasticity, Mol. Microbiol. 84 (5) (2012) 874–891.
[107] M. Radmacher, M. Fritz, C.M. Kacher, J.P. Cleveland, P.K. Hansma, Measuring the viscoelastic properties of human platelets with the atomic force microscope, Biophys. J. 70 (1) (1996) 556–567.
[108] H. Jin, X. Huang, Y. Chen, H. Zhao, H. Ye, F. Huang, X. Xing, J. Cai, Photoinactivation effects of hematoporphyrin monomethyl ether on Gram-positive and -negative bacteria detected by atomic force microscopy, Appl. Microbiol. Biotechnol. 88 (3) (2010) 761–770.
[109] J. Jenkins, J. Mantell, C. Neal, A. Gholinia, P. Verkade, A.H. Nobbs, B. Su, Antibacterial effects of nanopillar surfaces are mediated by cell impedance, penetration and induction of oxidative stress, Nat. Commun. 11 (1) (2020) 1626.
[110] T.P. Kohler, N. Gisch, U. Binsker, M. Schlag, K. Darm, U. Völker, U. Zähringer, S. Hammerschmidt, Repeating structures of the major staphylococcal autolysin are essential for the interaction with human thrombospondin 1 and vitronectin, J. Biol. Chem. 289 (7) (2014) 4070–4082.
[111] C. Rennemeier, S. Hammerschmidt, S. Niemann, S. Inamura, U. Zähringer, B. E. Kehrel, Thrombospondin-1 promotes cellular adherence of gram-positive pathogens via recognition of peptidoglycan, Faseb. J. 21 (12) (2007) 3118–3132.
[112] M. Herrmann, S. Suchard, L. Boxer, F. Waldvogel, P. Lew, Thrombospondin binds to Staphylococcus aureus and promotes staphylococcal adherence to surfaces, Infect. Immun. 59 (1) (1991) 279–288.
[113] C.C. Gomes, L.M. Moreira, V.J. Santos, A.S. Ramos, J.P. Lyon, C.P. Soares, F. V. Santos, Assessment of the genetic risks of a metallic alloy used in medical implants, Genet. Mol. Biol. 34 (1) (2011) 116–121.
[114] N.J. Hallab, M. Caicedo, A. Finnegan, J.J. Jacobs, Th1 type lymphocyte reactivity to metals in patients with total hip arthroplasty, J. Orthop. Surg. Res. 3 (1) (2008) 6.
[115] N.J. Hallab, K. Mikecz, C. Vermes, A. Skipor, J.J. Jacobs, Orthopaedic implant related metal toxicity in terms of human lymphocyte reactivity to metal-protein complexes produced from cobalt-base and titanium-base implant alloy degradation, in: Molecular Mechanisms of Metal Toxicity and Carcinogenesis, Springer, 2001, pp. 127–136.
[116] B.C. Costa, C.K. Tokuhara, L.A. Rocha, R.C. Oliveira, P.N. Lisboa-Filho, J. C. Pessoa, Vanadium ionic species from degradation of Ti-6Al-4V metallic implants: in vitro cytotoxicity and speciation evaluation, Mater. Sci. Eng. C 96 (2019) 730–739.
[117] M.A. König, O.P. Gautschi, H.-P. Simmen, L. Filgueira, D. Cadosch, Influence of vanadium 4+ and 5+ ions on the differentiation and activation of human osteoclasts, International journal of biomaterials 2017 (2017).
[118] E. Jia, X. Zhao, Y. Lin, Z. Su, Protein adsorption on titanium substrates and its effects on platelet adhesion, Appl. Surf. Sci. 529 (2020) 146986.
[119] X.-m. Meng, D.J. Nikolic-Paterson, H.Y. Lan, TGF-β: the master regulator of fibrosis, Nat. Rev. Nephrol. 12 (6) (2016) 325–338.
[120] G.J. Prud'homme, Pathobiology of transforming growth factor β in cancer, fibrosis and immunologic disease, and therapeutic considerations, Lab. Invest. 87 (11) (2007) 1077–1091.
[121] R.G. Triplett, M.E. Wong, Chapter 24 - efficacy of rhBMP-2 in association with dental implants, in: S.C. Bagheri, R.B. Bell, H.A. Khan (Eds.), Current Therapy in Oral and Maxillofacial Surgery, W.B. Saunders: Saint Louis, 2012, pp. 189–193.
[122] L. Chen, X. Lu, S. Li, Q. Sun, W. Li, D. Song, Sustained delivery of BMP-2 and platelet-rich plasma-released growth factors contributes to osteogenesis of human adipose-derived stem cells, Orthopedics 35 (9) (2012) e1402–e1409.
[123] Z. Mihaylova, R. Tsikandelova, P. Sanimirov, N. Gateva, V. Mitev, N. Ishkitiev, Role of PDGF-BB in proliferation, differentiation and maintaining stem cell properties of PDL cells in vitro, Arch. Oral Biol. 85 (2018) 1–9.
[124] S. Barrientos, O. Stojadinovic, M.S. Golinko, H. Brem, M. Tomic-Canic, Growth factors and cytokines in wound healing, Wound Repair Regen. 16 (5) (2008) 585–601.
[125] R. Bright, A. Hayles, J. Wood, N. Ninan, D. Palms, R.M. Visalakshan, A. Burzava, T. Brown, D. Barker, K. Vasilev, Bio-inspired nanostructured Ti-6Al-4V alloy: the role of two alkaline etchants and the hydrothermal processing duration on antibacterial activity, Nanomaterials 12 (7) (2022).